END-EFFECTOR COMPLIANCE INDEX FOR OPTIMIZING CABLE ANCHOR POINTS IN REDUNDANT CABLE-DRIVEN PARALLEL ROBOTS: DESIGN, CONSTRUCTION, AND CONTROL FOR CEMENT BASED ADDITIVE MANUFACTURING

A Thesis

by

Ahmet Burhan Kara

Submitted to the
Graduate School of Sciences and Engineering
In Partial Fulfillment of the Requirements for
the Degree of

Master of Science

in the
Department of Mechanical Engineering

Özyeğin University
September 2023

END-EFFECTOR COMPLIANCE INDEX FOR OPTIMIZING CABLE ANCHOR POINTS IN REDUNDANT CABLE-DRIVEN PARALLEL ROBOTS: DESIGN, CONSTRUCTION, AND CONTROL FOR CEMENT BASED ADDITIVE MANUFACTURING

Advisor: Asst. Prof. Özkan Bebek
Co-advisor: Assoc. Prof. Zeynep Başaran Bundur

Approved by:

Asst. Prof. Özkan Bebek, Advisor
Dept. of Mechanical Eng.
Özyeğin University

Asst. Prof. Ramazan Ünal
Dept. of Mechanical Eng.
Özyeğin University

Assoc. Prof. Kemalettin Erbatur
Faculty of Engineering and Natural Sciences
Sabancı University

Date Approved: 10 August 2023

To my Mother and my Father

ABSTRACT

This thesis presents a Cable-Driven Parallel Robot (CDPR) for additive manufacturing that has been designed, constructed, and controlled based on an introduced methodology for cable anchor point selection. The design and construction procedure of the CDPR was explained. The designed CDPR is a suspended type and redundantly actuated system. The robot comprises various components, including a frame for building the robot, cables connected to the end-effector, pulleys redirecting the cables to the end-effector from winches, winches for controlling cable length, an end-effector for printing, and an electrical panel to house electrical equipment. The cable tensions and stiffness of the end-effector were analyzed to achieve the desired size of the robot. To achieve this, the end-effector compliance index (ECI) was proposed to assess the stiffness of the end-effector within the workspace. This novel index uses cable direction vectors and cable lengths to determine the compliance of the given robot pose. Simulation results led to the development of a relation for obtaining an improved CDPR frame size, applicable to both suspended and constrained type CDPRs. Based on these simulations, a redundantly actuated suspended cable-driven parallel robot was constructed for a 1 m base length print part. Motion tracking experiments were conducted to assess the mobility and accuracy of the designed robot. The robot's working accuracy was evaluated by testing various printing paths. The experimental results verified that the developed system can achieve printing with an accuracy margin of less than 0.2%.

ÖZETÇE

Bu tez, kablo bağlantı noktası seçimi için tanıtılan bir metodolojiye dayalı olarak tasarlanmış, inşa edilmiş ve kontrol edilmiş, eklemeli imalat için bir Kabloyla Sürülen Paralel Robot (KSPR) sunmaktadır. KSPR'nin tasarım ve yapım prosedürü açıklanmıştır. Tasarlanan KSPR, askıya alınmış tipte ve artıksıl sınırlandırılmış olarak çalıştırılan bir sistemdir. Robot, robotu inşa etmek için bir çerçeve, son eğleyiciye bağlı kablolar, kabloları vinçlerden son eyleyiciye yönlendiren makaralar, kablo uzunluğunu kontrol etmek için vinçler, baskı için bir son eyleyici ve bir elektrik panosu dahil olmak üzere çeşitli bileşenlerden oluşmaktadır. Robotun istenen boyutunu elde etmek için son eyleyicinin kablo gerilimleri ve kararlılığı analiz edilmiştir. Bunu başarmak için, son eyleyicinin çalışma alanı içindeki kararlılığını değerlendirmek için son eyleyici uyumluluk indeksi (SUİ) önerilmiştir. Bu yeni indeks, verilen robot duruşunun uygunluğunu belirlemek için kablo yönü vektörlerini ve kablo uzunluklarını kullanır. Simülasyon sonuçları, hem askıya alınmış hem de kısıtlanmış tip KSPR'lere uygulanabilen, gelişmiş bir KSPR çerçeve boyutu elde etmek için bir ilişkinin geliştirilmesine yol açmıştır. Bu simülasyonlara dayanarak, 1 m taban uzunluğundaki bir baskı parçası için askıda artıksıl olarak kabloyla sürülen bir paralel robot inşa edilmiştir. Tasarlanan robotun hareketliliğini ve doğruluğunu değerlendirmek için hareket izleme deneyleri yapılmıştır. Robotun çalışma doğruluğu, çeşitli yazdırma yolları test edilerek değerlendirildi. Deneysel sonuçlar, geliştirilen sistemin %0,2'den daha düşük bir doğruluk payı ile yazdırmayı başarabildiğini doğrulamıştır.

ACKNOWLEDGEMENTS

This work was supported by the Scientific and Technological Research Council of Turkey (TUBITAK) under Grant No. 119M520.

TABLE OF CONTENTS

DEDICATION . . . . . **iii**

ABSTRACT . . . . . **iv**

ÖZETÇE . . . . . **v**

ACKNOWLEDGEMENTS . . . . . **vi**

LIST OF TABLES . . . . . **ix**

LIST OF FIGURES . . . . . **x**

I INTRODUCTION **1**

1.1 Motivation and Objective 5

1.2 Contribution of the thesis 6

1.3 Thesis Organization 6

II LITERATURE REVIEW **7**

2.1 Design of CDPRs 7

2.2 Control of CDPRs 8

2.3 Path Planning of CDPRs 11

2.4 Workspace of CDPRs 13

III MODELLING AND KINEMATICS **16**

3.1 Modelling of CDPR 16

3.2 Inverse Kinematics 18

3.3 Forward Kinematics 21

3.4 Anchor Point Correction 24

3.5 Tension Calculation 28

3.6 End-effector Compliance Index (ECI) 30

IV ANCHOR POINT SELECTION METHODOLOGY **33**

V RESULT OF SIMULATIONS **38**

VI IMPLEMENTATION OF CDPR DESIGN METHODOLOGY . 41

6.1 Case Study 41

6.2 Design and Construction of the CDPR 41

6.2.1 Robot Frame 42

6.2.2 Stainless-Steel Cables 44

6.2.3 Pulleys 45

6.2.4 Winch 48

6.2.5 End-Effector 49

6.2.6 Electrical Panel 51

6.3 Control of CDPR 52

6.3.1 Parameters of Servo Drivers 53

6.3.2 Motion Control 53

6.3.3 End-Effector Path Tracking Results 55

VII CONCLUSIONS 62

REFERENCES 64

VITA 70

LIST OF TABLES

LIST OF FIGURES

1 Schematic View of a 4 DoF CDPR 2
2 Schematic View of a 6 DoF CDPR 2
3 Schematic View of an 8 DoF CDPR 2
4 Wrench Feasible Workspace of FASTKIT 3
5 Planer Suspended and Constrained CDPR 4
6 Lower and Upper anchor point representation of a CDPR 17
7 Schematic Representation of Frame Assignments 17
8 Print Part with Suspended CDPR 18
9 Position Vector of Cables 21
10 Single Cable as the Radius of a Sphere 23
11 Top view of 4 sphere solution 23
12 Working Principal of Pulleys 25
13 Anchor Point Correction Schematic View 28
14 Zero ECI Schematic View 31
15 Maximum ECI Schematic View 32
16 ECI and mean tension vs half dimension of CDPR 35
17 ECI and mean tension vs half dimension of constrained CDPR 36
18 ECI and mean tension vs half dimension of suspended CDPR 37
19 Optimum CDPR base sizes for desired print parts 39
20 Constructed CDPR Frame 42
21 Upper and Lower pulleys and Single Corner of the Frame 43
22 Cross section of the 7x19 IWRC cable 45
23 Design of pulleys. 46
24 Machined pulley 47
25 Design of winches. 48
26 Machined winch 49
27 Machined End-Effector 50

28 Electrical Panel of the CDPR 52
29 Motion Capture with 7 Cameras 57
30 Circular Trajectory and Motion Capture Results 57
31 Close-up Circular Trajectory and Motion Capture Results 58
32 End-Effector Trajectory of Square and Circular Motion Respectively . 58
33 Square Trajectory and Motion Capture Results 59
34 Close-up Square Trajectory and Motion Capture Results 59
35 Trajectory result of the circular path and RMSE 60
36 Trajectory result of the square path and RMSE 61

CHAPTER I

INTRODUCTION

Cable-driven parallel robots (CDPRs) offer several advantages over other robotic systems. The main advantages of CDPRs are a large workspace, high accuracy, and high payload capacity [1, 2]. CDPRs consist of a series of cables that connect winches to the end-effector. According to the need of the robot, the actuation type can be under-constrained, exact-constrained, or over-constrained. For under-constrained robots, the number of cables is smaller than the DOF intends to control. These robots are used in applications that require the robot to have compliance such as rehabilitation or rescue operations [3, 4]. An under-constrained 4-cable robot can be seen in Figure 1. For exact-constrained robots, the number of cables is equal to the degree of freedom. These robots are used in applications that require robots to have full control over the pose of their end-effectors such as pick and place operations [5, 6]. An exact-constrained 6-cable robot can be seen in Figure 2. For over-constrained robots, the number of cables is higher than the controlled DOF of the robot. This allows the robot to have infinite cable tension solutions which increase the control over the pose of the end-effector [7, 8, 9]. An over-constrained 8-cable robot can be seen in Figure 3.

Depending on the application of a CDPR, the frame can be fixed to the ground or can be mobile. Mobile CDPRs (MCDPRs) have the ability to move cable anchor points attached to their end-effector [10]. FASTKIT [11] is an example of a mobile MCDPR which can be seen in Figure 4. FASTKIT is a mobile CDPR that is developed to ease item storage on warehouse shelves. By changing the position of the cars alongside a shelf, FASTKIT changes its workspace to reach different locations on the

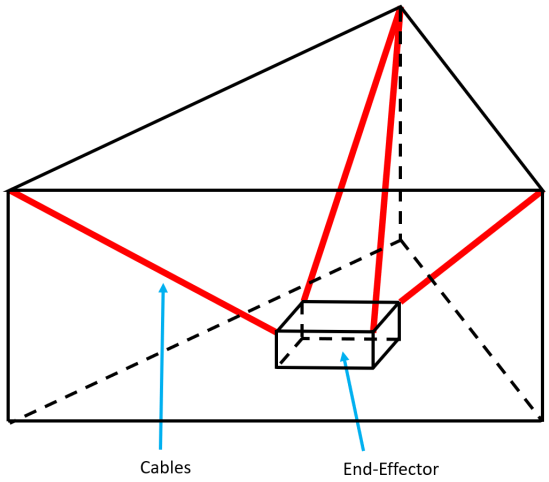

Figure 1: Schematic View of a 4 DoF CDPR

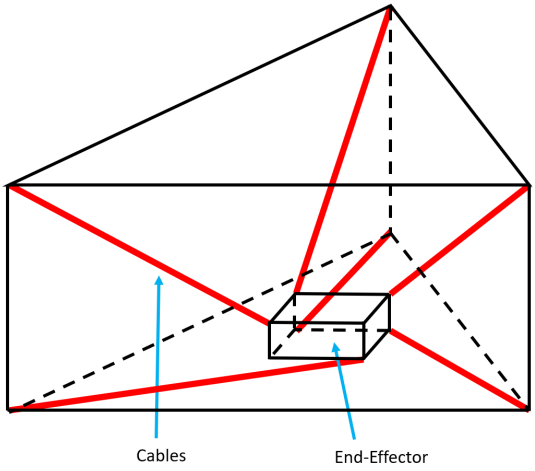

Figure 2: Schematic View of a 6 DoF CDPR

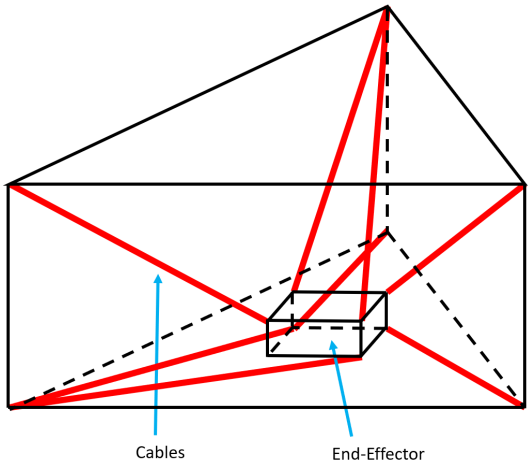

Figure 3: Schematic View of an 8 DoF CDPR

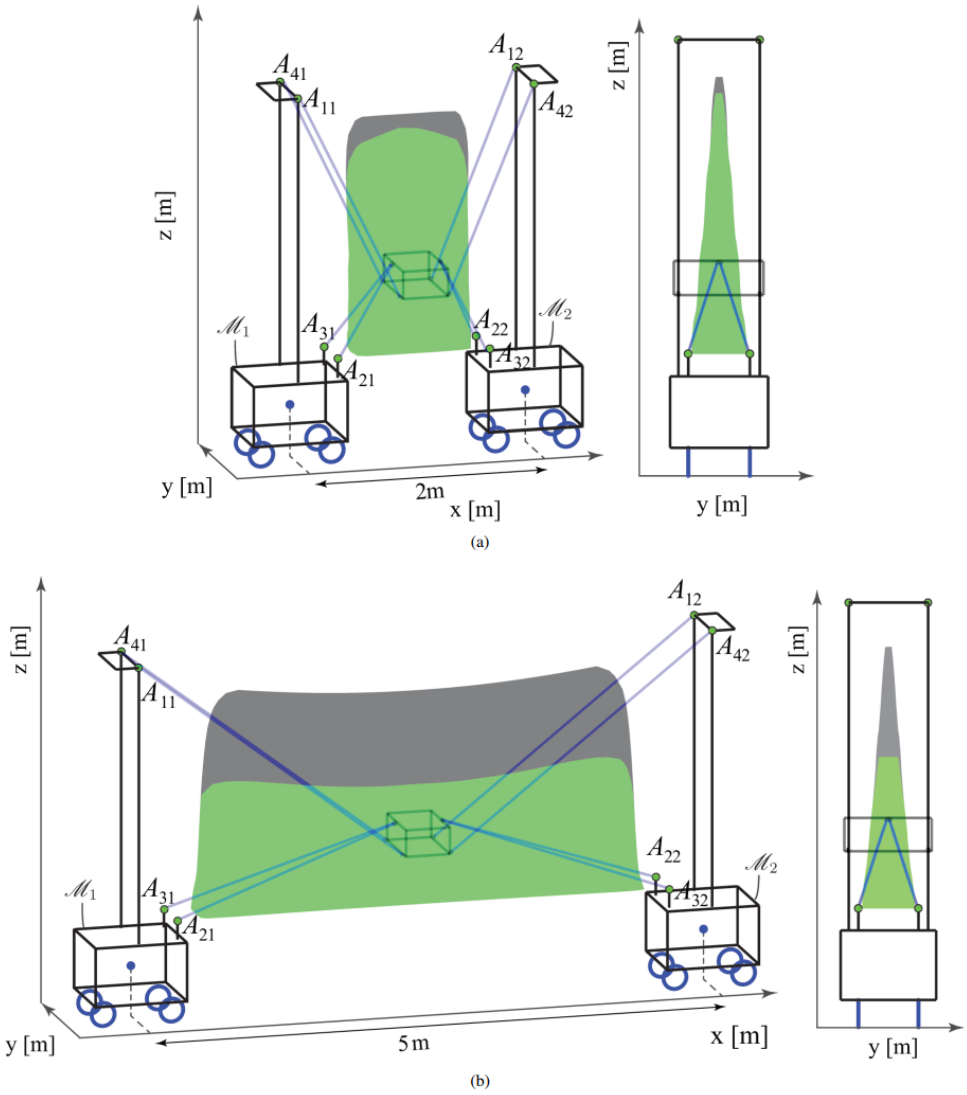

Figure 4: Wrench Feasible Workspace of FASTKIT [11]

shelves.

Also, there are two different attachment geometry types of end-effectors to the CDPR frame. One of the attachment geometry is suspended type where more space under the end-effector is created by placing all cables above the end-effector [12]. The other attachment geometry is the constrained type where some of the cable anchor points are placed below the end-effector to increase the stiffness of the CDPR [13]. To understand the attachment geometry better, the planer version of both

suspended and constrained type CDPR can be seen in Figure 5 respectively. For the suspended CDPR, the usable workspace is not affected by the cable collision with the environment. If there are some items on the workspace of the robot, the end-effector would collide with the items before the cables do. For the constrained CDPR, because the cables are attached to the bottom vertices of the CDPR's frame, the cables would collide if there are items in the workspace. On the other hand, the only thing that pulls the end-effector downward is the weight of it for the suspended CDPR. For the constrained CDPR, cables also can pull the end-effector downward. This phenomenon increases the control over the end-effector for the constrained CDPR.

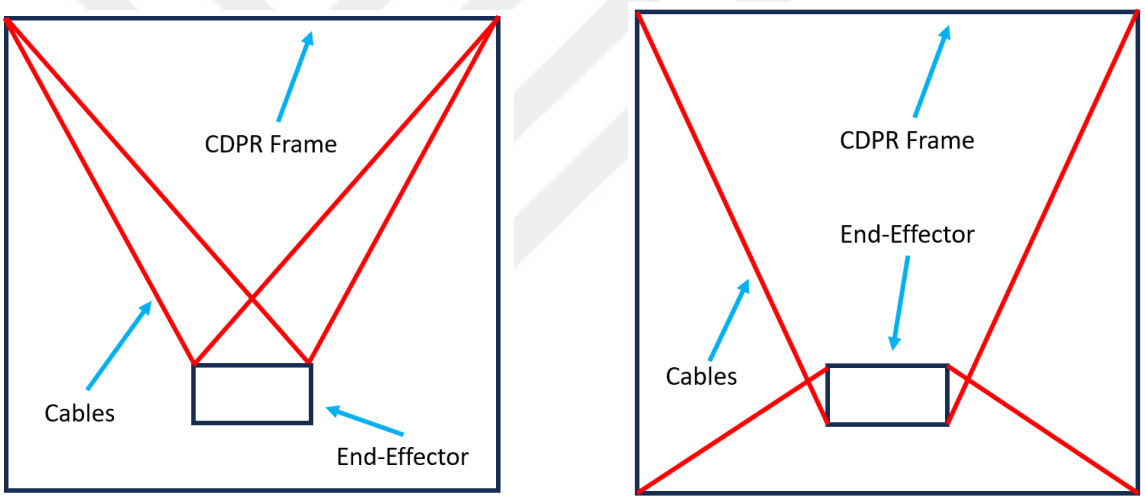

a) Planer Suspended CDPR b) Planer Constrained CDPR

Figure 5: Planer Suspended and Constrained CDPR

The task of a CDPR used in additive manufacturing is to move an extruder head attached to an end-effector along a pre-determined path and avoid contact with already printed material or the environment [14]. For successful results, the CDPR's working area should be wider than the part to be printed. Longer cables are required to create a wider workspace. However, long cables reduce the stiffness of the end-effector due to being more sensitive to external forces [15]. The stiffness of the end-effector influences the quality of the printed part [14]. CDPRs with smaller working areas, that is using shorter cables, provide higher stiffness and better print quality.

Though, short cables require higher cable tensions for task completion [16].

As with all manufacturing devices, it should always be aimed to design a low-cost CDPR. Higher cable tensions would increase the manufacturing cost of the robot [2]. Therefore, the length and tension of the cables should be optimized to achieve an acceptable print quality and a low-cost robot. Each part to be printed requires a unique set of poses (unique workspace), depending on its size and geometry. The CDPR size should be chosen based on the size of the part to be printed for optimal results.

1.1 Motivation and Objective

In recent years, the field of robotics has witnessed remarkable advancements, and cable-driven parallel robots (CDPR) have emerged as a compelling new class of robots offering distinct advantages. CDPR robots exhibit high payload capacity, adaptability, and accuracy, making them well-suited for various applications, including manufacturing, medical treatments, maintenance, pick and place operation, and space exploration. However, despite their promising attributes, CDPR robots still encounter challenges and design constraints that hinder their full utilization and potential.

There is not enough research that looks at the trade-off between the stiffness of an end-effector and the cable tension in cable-driven parallel robots (CDPR) in the literature. Despite the unique advantages of CDPR robots in terms of payload capacity, flexibility, and accuracy, reaching the ideal stiffness while maintaining the proper cable tension levels is essential for their effective operation.

Taking these observations into account, this thesis presents a methodology for identifying the balanced cable anchor points on the frame of a fixed-based redundantly actuated CDPR for use in additive manufacturing. The methodology aims to not only increase print quality by increasing the stiffness of the end-effector but also lower the build cost of the CDPR by lowering cable tensions. Then, by using the presented

methodology, a cable-driven parallel robot has been designed and the design process has been explained. Then, the designed cable-driven parallel robot has been built and the building process has been explained. Lastly, the control of the built robot has been done, and the control process has been explained. The robot's experimental path-tracking results were presented.

1.2 Contribution of the thesis

The work presented in this thesis aims mainly to locate the cable anchor points of a cable-driven parallel robot. The method used in this thesis is different than the other existing anchor point optimization methodology in the fact that the method uses purely geometrical properties of the cable-driven parallel robot and the end-effector pose. The methodology uses an index called End-Effector Compliance Index (ECI) which is introduced in this thesis. By using the ECI, the stiffness of the end-effector due to the geometry of the CDPR can be quantified. ECI can be used before applying any control algorithm on the end-effector. Therefore, it is a powerful methodology to use for the initial design. Also, calculating ECI requires only inverse kinematics of the CDPR which is relatively easy to calculate.

1.3 Thesis Organization

This thesis is structured as follows: Section II presents the literature review. Modeling and kinematics of the cable-driven parallel robot (CDPR) were explained in Section III. Anchor point selection methodology and the results of the simulations were written in Section IV and Section V respectively. Section VI explains the implementation of the CDPR design methodology. Lastly, the Conclusion was presented in Section VII.

CHAPTER II

LITERATURE REVIEW

2.1 Design of CDPRs

Several concepts related to the geometry optimization on CDPRs were introduced in [17] which are cable collision, workspace analysis, and cable connection combination on an end-effector. Workspace analysis was further studied in [18, 19]. Also, cable configuration was studied in [20] to increase the rotational range of the end-effector. An algorithm was suggested by [14] to optimize the rigidity and printing space of a fully constrained CDPR by changing the coordinates of anchor points on the end-effector.

The geometry selection of a redundantly actuated, cable-suspended parallel robot with heavy load and wide workspace capability is introduced in [18]. Geometry selection refers to the cable drawing points on the base and cable attachment points on the mobile platform. A CDPR has been built to demonstrate these capabilities. Moreover, a CDPR that can be used to automate the final large-scale assembly of solar panels in the field is introduced in [21]. Additionally, a new cable configuration analysis to increase the rotational range of suspended 6-DOF CDPRs is presented in [5]. CDPRs have larger workspaces when end effectors only translate, but their workspaces decrease substantially when end effectors also rotate. The paper examines different cable configurations to increase the rotational workspace, showing that the workspace of suspended six-DoFs CDPR is increased.

Additionally, the effect of springs on the wrench and different parameters are investigated in [5]. Since cables cannot push, attachment points on the moving platform are a challenge to satisfy the design requirements. Therefore, redundant cables

or loads on the moving platform are used. In this paper, springs are used, and it is observed from the experiments that the springs can increase or reshape the WFW. Furthermore, cable guiding mechanisms (CGMs) are directly related to the reconfigurability of CDPRs. However, the complicated kinematic model of pulley-based CGMs makes velocity and acceleration mappings unknown. [22] establishes an analytical and compact model for CGM. This model can derive velocity and acceleration mapping from the moving platform. Continuities of cable trajectory and tension are provided, and the exact identification of Jacobian and its derivative is formulated. The method and formulations are verified by simulations and experiments on a redundant CDPR.

Design optimization of a spatial four-cable under-constrained CDPR for rapid lifescan is studied in [23]. A gyro sensor is used to compute the configuration of the robot in real time, and a new approach to solving forward kinematics is provided using intersection points of spheres. Additionally, an omnidirectional aerial manipulator attached to a suspended CDPR with a spring is introduced in [24]. Omnidirectional aerial vehicles can be used for dexterous manipulation tasks, but their efficiency is low due to gravity compensation. The aim is to use CDPR to compensate for the energy losses due to the gravity of the aerial manipulator.

2.2 Control of CDPRs

The stiffness of constrained CDPRs can be altered by controlling cable tensions[7]. With high tension values, the end-effector will have higher stiffness. For suspended CDPRs, gravity is utilized to maintain tension in the cables [9]. Practically, suspended CDPRs cannot have higher stiffness by increasing cable tensions due to all cable forces being against gravity. For the same reason, suspended CDPRs can carry heavier loads than constrained CDPRs. In addition, CDPRs that are redundantly actuated, using a greater number of active cables than degrees of freedom (DOF), offer increased

stiffness, larger workspaces, and the ability to customize workspace geometry [25, 26]. Redundantly actuated CDPRs can alter the stiffness of the end-effector by changing cable tensions [7].

The static model and stability of static equations for CDPRs with less than 6 cables in a crane configuration are introduced in [3]. The method uses ordinary linear-algebraic equations and provides examples of CDPRs that has cable numbers ranging from 2 to 4. However, this method might not be feasible for 8 cables with 6 DoFs due to redundancy and the increased complexity of the equations. Additionally, static analysis of CDPRs with non-negligible cable mass to compute the static displacement of a homogeneous elastic cable is introduced in [27]. The result is used to solve inverse kinematic equations, achieving sag-induced stiffness of the cables. Two large CDPRs have been analyzed, and the results demonstrate that cable sagging has significant effects on both stiffness and inverse kinematics. Moreover, a new method of static analysis of CDPRs with inextensible and non-negligible mass cables is introduced in [28]. Also, more advanced control algorithms were introduced such as the optimal tension distributing model developed in [29] and the real-time capable algorithm was presented in [30].

Redundancy resolution of feasible and continuous cable tension distribution along a trajectory of n-DoFs CDPR with n+2 cables is introduced in [31]. The algorithm used in this paper can be easily modified to determine the optimal cable tension distribution. The algorithm is found to be efficient and can be used in real-time, even in the worst-case scenario. This paper also reports results for two different 6-DoF CDPRs. Additionally, a novel linear-programming formulation for optimally safe tension distribution for CDPRs with a slack variable is introduced in [32]. This slack variable can be used for the explicit computation of a feasible, near-optimal starting point, allowing rapid computation of optimally safe tension distribution. Two static simulation results that avoid tension limits and a real experimental result from a

CDPR are also presented.

An auto-calibration method is implemented on an over-constrained CDPR using internal position sensors located in the motors, as studied in [33]. A calibration workflow is proposed and implemented, simulated, and applied to an actual CDPR. Furthermore, a calibration sensor device and an auto-calibration methodology are introduced for over-constrained CDPRs using a one-dimensional laser distance sensor attached to a robotic arm in [34]. The accuracy of the experimental setup is 0.92mm.

The stiffness matrix of a CDPR with hefty cables is derived analytically, and the homogenization of the stiffness matrix is introduced in [5]. Also, stiffness analysis of DCPRs, including static and dynamic stiffness, is analyzed in [35]. The cable models include cable mass and elasticity. Based on these models, static stiffness is related to end effector pose error, and dynamic stiffness is related to robot natural frequencies. A 6-DoF CDPR is used for simulations and experiments, and other methods available in the literature are compared. The results show the importance of cable mass and elasticity.

Additionally, an interactive control approach to prevent cable interference and preserve the geometry of the cable mechanism is explained in [36]. In this approach, the controller generates a repulsive force to prevent any cable crossing, and the distance between cables is computed using the Krush-Khun-Tucker condition.

A general model to increase stiffness and minimize undesired perturbations under external disturbances on redundant and kinematically-constrained CDPRs is introduced in [26]. However, this study might not be valid for CDPRs that are not kinematically constrained and in a suspended configuration. Also, decoupled active canceling vibrations of CDPRs with lightweight cables in the model space are introduced in [37]. CDPRs can have very big workspaces with light parts and less energy. However, this results in cable sagging and low stiffness, causing disturbance vibration

and position errors. In the model space, vibrations are separated into orthogonal signals, allowing SISO control methods to cancel the vibrations. The proposed method is tested on an 8-cable, 6-DoFs CDPR and on a simulation. Additionally, CDPRs with m cables that deform under their own mass and elasticity are studied in [38]. Inverse kinematics requires a square system of equations, and inverse kinematics with an under-constrained system cannot be solved using conventional methods. In this study, an algorithm is proposed to solve under-constrained CDPRs' inverse kinematics and forward kinematics. A generic algorithm for solving forward kinematics for any number of cables is proposed, and the method is used on an 8-cable CDPR's inverse kinematics and forward kinematics.

2.3 Path Planning of CDPRs

A path-planning method that regulates cable tension within accepted cable tension boundaries is proposed in [39]. The method attempts to counteract any wrench in a predefined uncertainty region. Also, continuous dynamic path motion planning for a 3-DoFs spatial suspended robot is proposed in [40]. The path consists of 3 points, which are then connected using quintic polynomials to enhance the dynamic performance. Additionally, the optimum configuration of superfluous cables in redundant planar suspended robots for minimum time trajectory is investigated in [8]. The limitation on cable tension and cable velocities are considered for calculating acceleration and velocity along the path. Using a genetic algorithm and bang-bang control, the optimum superfluous cable configuration and switching points are obtained.

A dynamic trajectory planning method for a point-to-point motion of a three-DoFs suspended CDPR is introduced in [41]. Natural frequencies and associated periodic trajectories, which can be found by integrating the dynamic model, are used to design trajectories that can connect consecutive points lying beyond the static workspace. The method ensures zero velocity at each target point and continuity of acceleration.

Also, a dynamic trajectory planning technique for six-DoFs suspended CDPR is introduced in [6]. The paper presents mathematical models and imposes restrictions using the tilt-and-torsion angle convention for the rotational component of the trajectories. Dynamic differential equations, which are linear under some conditions, are used for the translational component of the trajectories.

A trajectory solver procedure is explained in [42]. This solver uses the moving platform's current position and velocity orientation, along with the goal position and goal velocity orientation, to choose one generated primitive interconnecting path. The cycle repeats until the moving platform reaches the goal position. Simulation experiment results are presented. Also, trajectory planning for the prescribed motion time and path geometry of an underactuated CDPR is presented in [4]. The study proposes a novel trajectory planning algorithm that works by tracking the constrained geometric path in a specified time, allowing transitions between stable static poses of a three-cabled 6-DOF CDPR. Constraints on position and velocity at the beginning and the end of the motion are made, and the problem is dealt with as a boundary value problem.

IPAnema is presented in [43]. Dynamic equations of the mobile platform, pulley kinematics, and linear spring-based cable models are implemented. The model can be used in real-time, controller design, high-dynamic, and large-scale robot applications. Also, a 3-D cable robot called NIMS3D for sensing applications is presented in [44]. Hardware components, installation procedure, kinematic and dynamic analysis, and description of control methods are explained, along with experimental results. It is shown that energy efficiency can be improved by using optimized parabolic trajectories. Additionally, an efficient new task-optimized technique with parallel computing through OpenMP directives is introduced in [45]. The method uses the differential evolution algorithm, and its intrinsic parallelism is exploited using OpenMP directives to evaluate the manipulator's associated reachable and wrench workspaces. The

algorithm increases performance by 7.4 times.

2.4 Workspace of CDPRs

Furthermore, cables can balance any external wrench, which forms a set of poses called WFW (Wrench-Feasible Workspace). The theorems characterizing the poses of WFW are proposed in [13], and they are used to disclose the part of the reachable workspace. An efficient algorithm that determines the constant orientation cross-section is also introduced. Additionally, a new method called Twist Feasible Workspace (TFW) is presented in [46] to analyze the workspace of a CDPR. A pose can be said to be TFW if it satisfies a range of linear and rotational velocities while staying within desired cable speed limits. TFW is basically WFW but is interested in not imposing torque on the moving platform but focusing on the velocities of the moving platform. TFW can be used to optimize actuators and winches.

A method for avoiding configurations that might cause instability due to internal loads or external forces is studied in [47] for 3-DoF cable-driven mechanisms (CDMs). The idea is to prestress the stable Wrench-Feasible Workspace (WFW) to increase the overall stiffness of the mechanism. A genetic algorithm is used to optimize the geometry of a CDPR with 4 cables to achieve the desired PSWCW (Prestressed Wrench-Feasible Workspace). The results may guide the preliminary selection of mechanism dimensions and cable connections.

The wrench-feasible workspace (WFW) for CDPRs, which have more cables than degrees of freedom, is introduced in [48]. This work utilizes geometric methods to determine the boundary of WFW instead of testing a cloud of points of possible WFW. In today's world, there might be no need for this method due to the increased availability of computational power in workstations. Additionally, the study in [49] focuses on determining the base anchor points that satisfy external wrenches and enable a no-collision path. The aim of this paper is to explain the method used

to transport proper tools for painting around offshore structures. The investigation involves a simplified structure with 4 tubes, which is analyzed using a constrained suspended CDPR. In addition, [50] presents a workspace analysis of planar and spatial planar CDPRs using linear algebra for upper cable tension limits and a variant of Bland's pivot rule to calculate the workspace.

The relationship between the boundary of the workspace and the cable configuration of a CDPR in an environment that has obstacles is studied in [51]. Conditions under which a CDPR is valid are examined. Also, [52] proposes a methodology to trace the wrench-feasible workspace. Reconfigurable CDPR robots can change their geometry, and a novel concept of a reconfigurable CDPR attached to multiple mobile bases is called Mobile CDPR. The available wrench set depends on cable tension limits and the static equilibrium condition of mobile bases. The available wrench set is constructed by a convex hull approach and hyperplane shifting method.

The tension factor (TF) reflects the reflective cable tension distribution, and for redundant cables, the TF values are not unique. [53] shows that using a linear optimization approach, the optimized workspace can be found. A global tension index, which can be achieved by integrating local TF, is proposed to evaluate the quality of the workspace. Moreover, a cable-driven planar robot with a tilting working plane is explained in [54]. The robot has a moving pulley block that allows high-force capabilities. The design, kinematics, and control of the device are presented with experimental results.

For the first time, singularity analysis using the Irvine model on CDPRs is introduced in [55]. The mathematical model of singularity analysis is presented, and both inverse kinematics and forward kinematics have a singularity called parallel robot singularity, which is equivalent to parallel robots with rigid legs. Another singularity called full singularity is examined and occurs when two of the inverse kinematics and forward kinematics solution branches intersect. An algorithm is presented to

prove that singularity exists and estimate the location with arbitrary accuracy. The combined singularity cannot be determined. Additionally, CDPRs have a limited orientation workspace due to cable interference and collisions between cables and surroundings. A 4-DoFs planar under-constrained CDPR with an articulated moving platform is studied in [56]. The end effector is articulated through a cable loop, which enables unlimited, singularity-free orientation and a large translational workspace. However, some unwanted rotational motions of the moving platform arise, parasitic inclination, due to the cable loop. Also, cable and cabin structures are compared with the Steward platform, and the force singularity of the cabin and cabin system is explored by using the force transformation matrix in [57]. To eliminate the singularity, one more cable is added to the system.

CDPRs have low moving inertia and provide high-speed motion. Cable tension is related to the synchronization motion relation between cables, which is often omitted. [58] proposes two synchronization controllers to increase tracking accuracy. The controllers guarantee asymptotic convergence to zero for both tracking errors. Experiments are done on a three-DoF CDPR. Also, the accuracy of cable-driven robots needs to be improved since they use soft links. [59] deals with the stability analysis of cable-driven robots using a vision-based controller. Analytical models and the experimental setup are provided with two CDPR examples.

CHAPTER III

MODELLING AND KINEMATICS

In this chapter, the modeling of a CDPR, its kinematic equations, and cable tension calculation methodology is presented and also the End-effector Compliance Index (ECI) is introduced. In design calculations, the effects of the robot dynamics are neglected assuming that the printing path would not require sharp turns and the printing head would move with constant velocity. Cable mass, cable sagging, and friction have an effect on control performance. However, to simplify the study, they are neglected in modeling and simulations. The inverse kinematics solution was used to find the position of the end-effector.

Also to limit the research scope about the shape of the CDPR, it is taken as a half-cube. Meaning that the height of the CDPR frame is half of the base lengths. This half-cube shape is suitable for most of the printing operations since the shape of most print parts can be modeled as half-cubes.

3.1 Modelling of CDPR

Schematic representation of a CDPR with frame assignments and cable attachment points is represented in Figure 7. The base and end-effector of the CDPR and the representation of a single cable and its attachment points are shown. Cable attachment points on the base, also known in the literature as the anchor points, are represented with b_i. The other ends of the cables are represented with e_i. The cables are represented with r_i where $i = 1, 2, \ldots, n$. n is the number of active cables. In this work, the CDPR is redundantly actuated having two additional actuators. The robot's DOF number is denoted by m which is 8.

The attachment configuration of cable to the end-effector is selected so that the

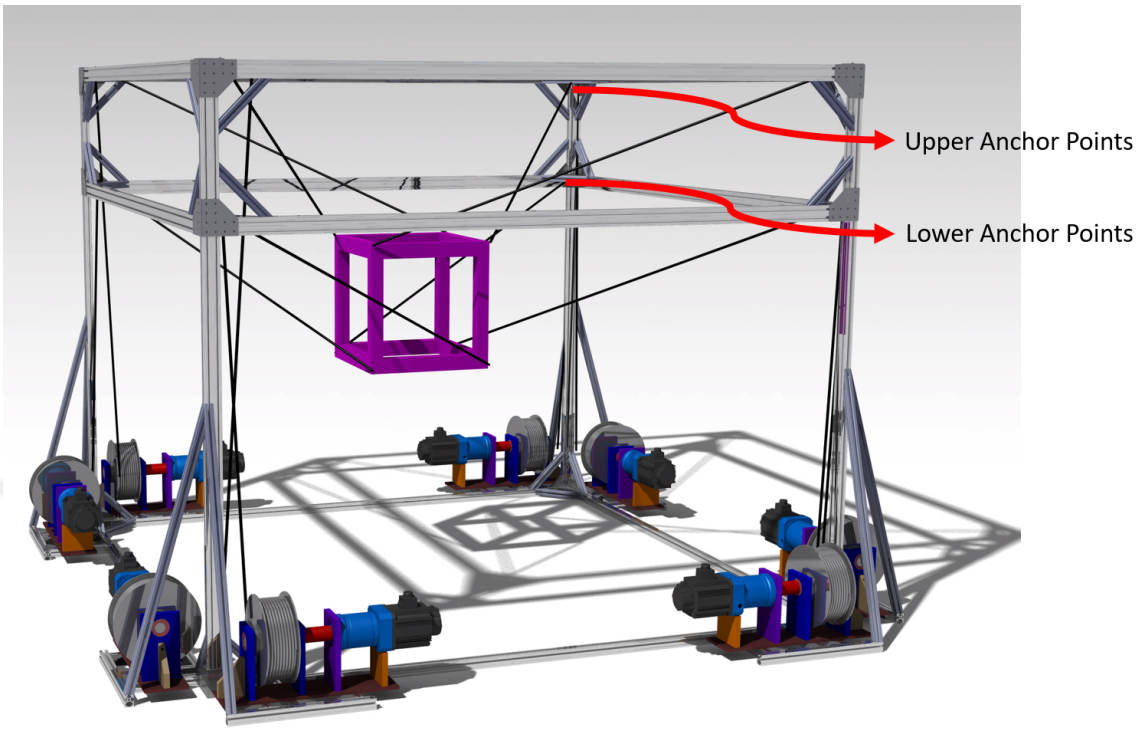

Figure 6: Lower and Upper anchor point representation of a CDPR

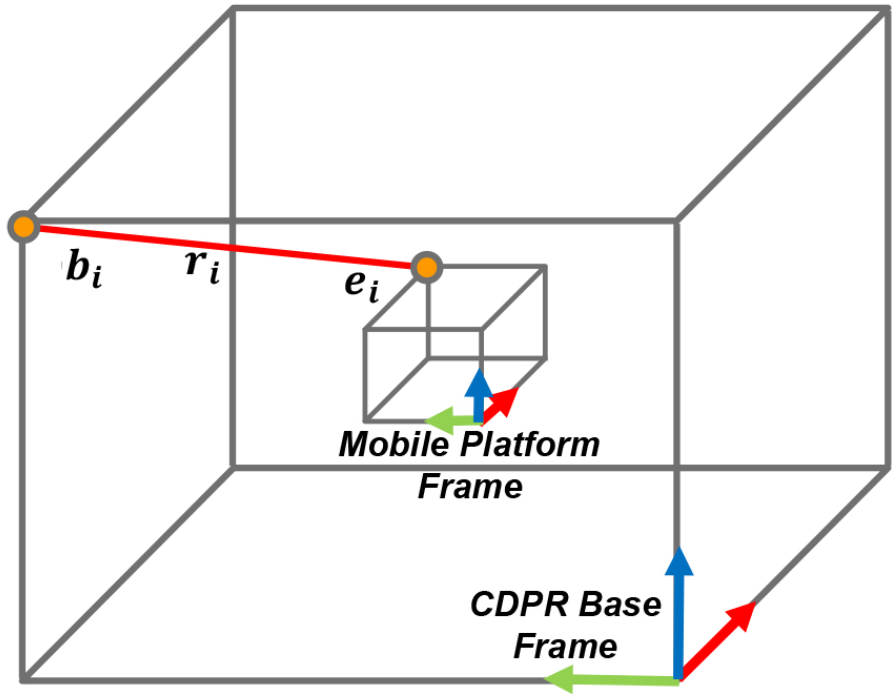

Figure 7: Schematic Representation of Coordinate Frame Assignments on the CDPR

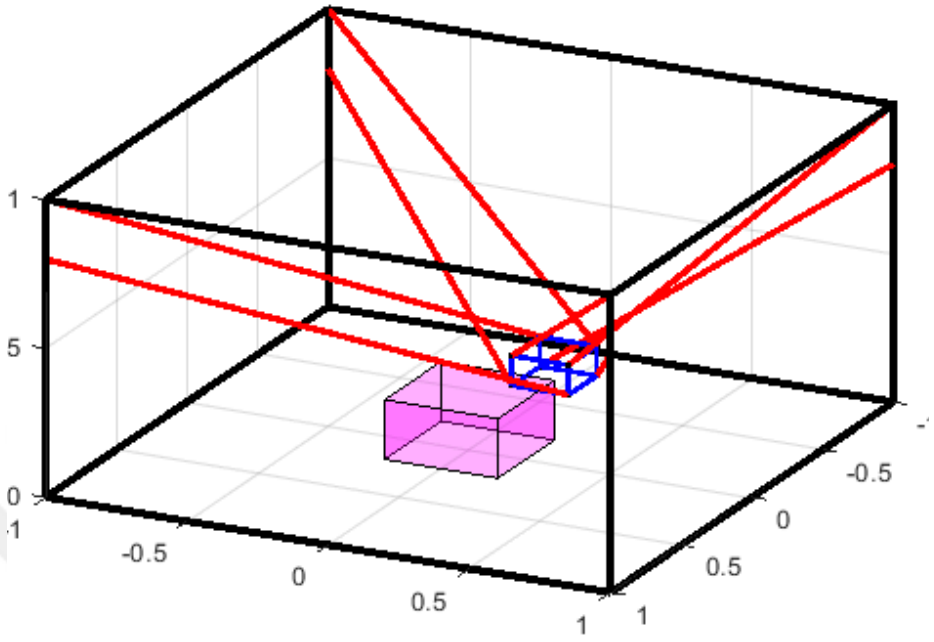

Figure 8: Demonstration of a printed half-cube piece with a base size of 0.4 m and a suspended CDPR featuring a 1 m half-length frame

rotational range of the platform is increased, similar to the one presented in [20]. In this configuration, cables are divided into 2 sets and are attached to the lower anchor and upper anchor points of the base (shown in Figure 6). The anchor points of each set are leveled the same. Cables attached to the upper anchor points are attached to the upper vertices of the mobile platform. Cables attached to the lower anchor points are attached to the lower vertices of the mobile platform. Upper cables are attached to the second closest vertex in the clockwise direction (as shown in Figure 7). Similarly, lower cables are attached to the second closest vertex in the counterclockwise direction.

3.2 Inverse Kinematics

Given a desired end-effector location and orientation (or pose) in space, inverse kinematics is a mathematical technique used in robotics and computer graphics to predict

the joint configurations (angles or positions) of a robotic arm or an articulated figure. In simpler terms, it is the process of determining the joint angles or coordinates required to position a robotic arm or a character's limb at a certain end-point and orientation. For tasks like motion planning, where a robot should reach a specific location or manipulate objects in a certain way, inverse kinematics is crucial in robotics. Inverse kinematics is frequently utilized in a wide range of situations where precise control and realistic movements are required, such as robot arm control, computer animation, virtual reality, video games, and simulation.

For cable-driven parallel robots (CDPRs), inverse kinematics is essential for determining the cable lengths required to achieve the desired end-effector position and orientation. Tensioned cables are used in CDPRs to link the base and movable platform. Due to the non-linear correlations between cable lengths and end-effector posture, solving the inverse kinematics problem is challenging and calls for complex mathematical techniques. Accurate solutions are crucial to support applications in aerial manipulation, pick-and-place operations, and precision movements, enabling effective motion planning and control in CDPRs. The relevance of CDPRs in contemporary robotics and automation is anticipated to grow with continued development and practical use.

A homogeneous transformation matrix, T_i, for the ith cable attachment point on the end-effector with respect to the end-effector frame is formed, (1), to derive the inverse kinematics of the system.

$$T_i = \begin{bmatrix} R_R(a)\, R_P(b)\, R_Y(c) & 0 \\ 0 & 1 \end{bmatrix} \begin{bmatrix} I & c_i \\ 0 & 1 \end{bmatrix} \tag{1}$$

where, $R_R(a)$, $R_P(b)$, and $R_Y(c)$ are 3×3 the rotation matrices of roll, pitch, and yaw orientations, respectively. a, b, and c are the rotation angles of the end-effector about the $x-$, $y-$, and $z-$axes, respectively. I is 3×3 identity matrix. c_i is 3×1 ith

cable attachment point on the end-effector with respect to the end-effector coordinate frame.

Using these transformation matrices, it is possible to get the cable attachment locations relative to the end-effector coordinate frame. These locations can be converted to the CDPR base coordinate frame by adding the coordinate of the end-effector relative to the CDPR base coordinate frame.

$$\begin{bmatrix} e_{x,i} \\ e_{y,i} \\ e_{z,i} \end{bmatrix} = \begin{bmatrix} x \\ y \\ z \end{bmatrix} + \begin{bmatrix} T_i(1,4) \\ T_i(2,4) \\ T_i(3,4) \end{bmatrix} \tag{2}$$

where, $T_i(1,4)$, $T_i(2,4)$, and $T_i(3,4)$ are the x, y, and z coordinates of the ith cable attachment point on the end-effector with respect to the end-effector coordinate frame. x, y, and z are the position of the end-effector with respect to the base frame. $e_{x,i}$, $e_{y,i}$, and $e_{z,i}$ are the x, y, and z coordinates of the ith cable attachment point on the end-effector with respect to the CDPR base frame.

Also, the attachment points of the cables are known on the frame. By finding the distance between the cable connection points between the frame and the end-effector, cable lengths can be found.

$$\mathbf{d}_i = \begin{bmatrix} b_{x,i} \\ b_{y,i} \\ b_{z,i} \end{bmatrix} - \begin{bmatrix} e_{x,i} \\ e_{y,i} \\ e_{z,i} \end{bmatrix} \tag{3}$$

where $\mathbf{d}_i$ is the position vector of ith cable's two endpoints which can be seen in Figure 9. In other words, d_i is the length of the ith cable. $b_{x,i}$, $b_{y,i}$, and $b_{z,i}$ are the ith cable's coordinates with respect to the base frame. The magnitude of $\mathbf{d}_i$ represents the length, r_i, of the the ith cable:

$$r_i = \|\mathbf{d}_i\| \tag{4}$$

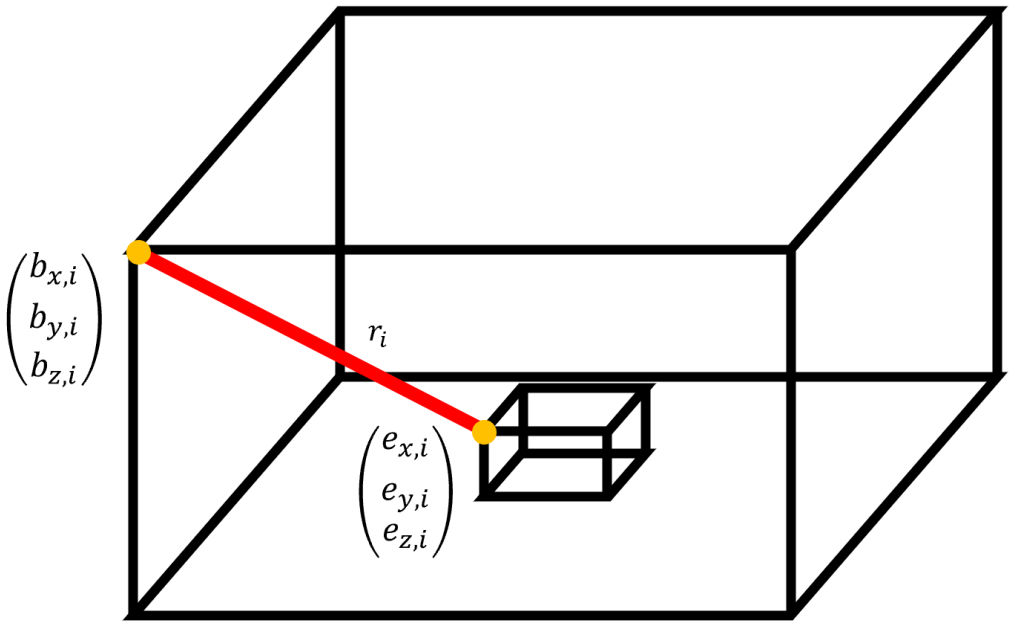

Figure 9: Position Vector of Cables

3.3 Forward Kinematics

The calculation of the position and orientation of the end-effector (such as the tool or hand) of a robotic arm or an articulated figure, given the joint angles or coordinates of the robot's individual segments or links, is known as forward kinematics. It is a fundamental concept in robotics and computer graphics. To put it simply, forward kinematics is the process of figuring out the end-effector's location in space based on the known joint angles or joint locations. By considering the existing arrangement of the robot's joints, it enables us to determine the end-effector's location and orientation.

Depending on the type of robot or articulated figure being studied, forward kinematics is relatively straightforward and involves calculating a series of transformation matrices or equations. This information is crucial for activities like motion planning, path development, and visualizing the robot's movement in a specific workspace. On

the other hand, inverse kinematics is the process where we determine the joint angles or coordinates required to achieve a specific end-effector position and orientation. In contrast, forward kinematics calculates the end-effector's location based on joint angles or coordinates.

The primary difference between serial and parallel robots, in terms of forward kinematics, lies in the way they are built and how they move. Parallel robots have multiple joints arranged in parallel, as opposed to serial robots, which have a single chain of joints. In general, solving the forward kinematics for serial robots is easier than for parallel robots because of the interaction between multiple legs.

Forward kinematic equations are used to find the position and orientation of the end effector from the cable lengths controlled by the motors. To find the forward kinematic equation, cable lengths and/or motor angular positions are required. With a known cable length and known attachment point on the frame, the free end of the cable can be found at any point on a surface of a sphere. This sphere is located at the cable attachment point on the CDPR frame. The radius of the sphere is the cable length. Therefore, cables can be modeled as a line from the center to the surface of spheres [60]. The position of a free end of a cable can be found by using the general sphere formula which can be written as (5).

$$(x_i - h_i)^2 + (y_i - k_i)^2 + (z_i - l_i)^2 = {r_i}^2 \tag{5}$$

Where x_i, y_i, and z_i are the center coordinates of the spheres. h_i, k_i, and l_i are possible coordinates of the surface of the sphere. r_i is the radius of the sphere. A cable as the radius of a sphere centered at an anchor point on the CDPR frame can be seen in Figure 10. To find the pose of the end-effector, 6 equations must be solved together to find 3 positions and 3 orientations of the end-effector. However, because cables are not attached at a single point on the end effector, their general sphere equations do not have the same solution. To make the solution the same, virtual sphere centers

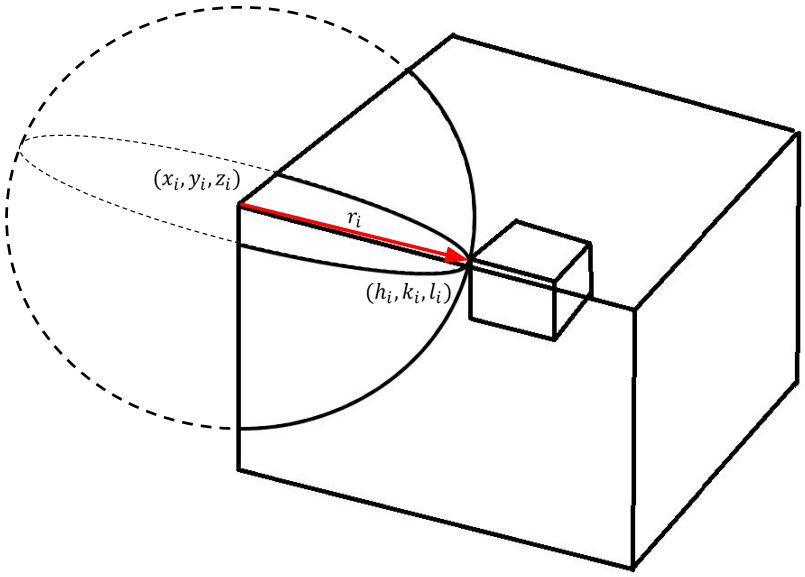

Figure 10: Representation of a single cable as the radius of a sphere centered at an anchor point on a CDPR frame.

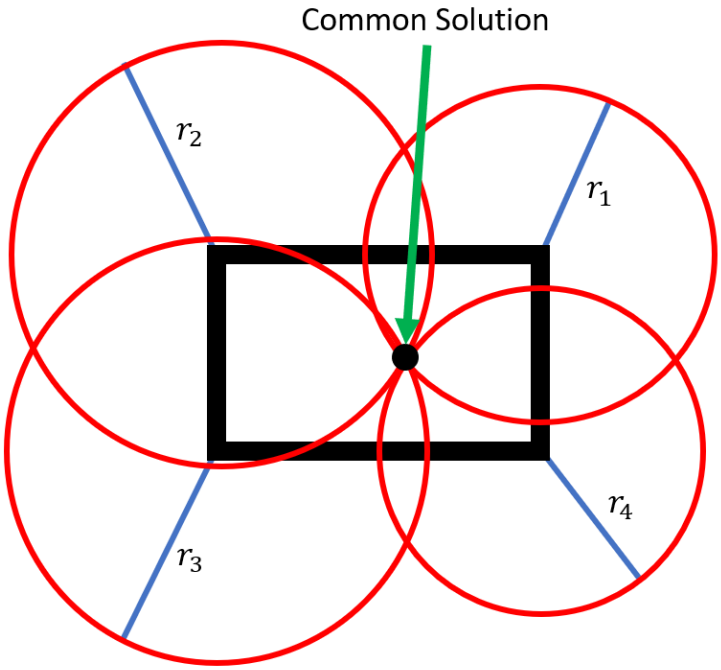

Figure 11: Top view of 4 sphere solution

are used. One cable is selected as a master point. The other 5 cables were translated such that their attachment location on the end-effector coincide. Therefore, all cable virtually intersects at a single point and have a common solution. Then, these 6 equations for 6 cables can be solved simultaneously to calculate 3 positions and 3 orientations values for the end-effector. The top view of the 4-sphere solution can be seen in Figure 11.

3.4 Anchor Point Correction

In the inverse kinematics calculations, cable attachment points on the robot's frame are fixed. However, there are pulleys that re-direct the cables from winches to the end effector. These pulleys can be seen in Figure 12. According to the position of the end effector, the cable break-out points on the pulleys change. Also, because of the circular design of the pulleys, cable break-out points shift inside the workspace. Therefore, cable anchor point correction is required.

Pulleys are designed to rotate on an axis that is tangent to the anchor points on the pulleys. In this way, when pulleys rotate, the cable part between the winch and the pulley does not change, see Figure 12. In the anchor point correction calculation, the anchor point is selected as the place where the cable's first contact point is on the pulley. Then according to the position of the end effector, the cable break-out point was calculated. To understand the concept better Figure 13 can be seen. After finding the cable break-out point, the cable around the pulley and the cable between the break-out point and the end-effector can be calculated by the following set of equations:

$$AC_{1,i} = b_{z,i} - e_{z,i} \tag{6}$$

The vertical distance from the anchor point to the end-effector attachment point for the ith cable can be found by subtracting them which is denoted as $AC_{1,i}$.

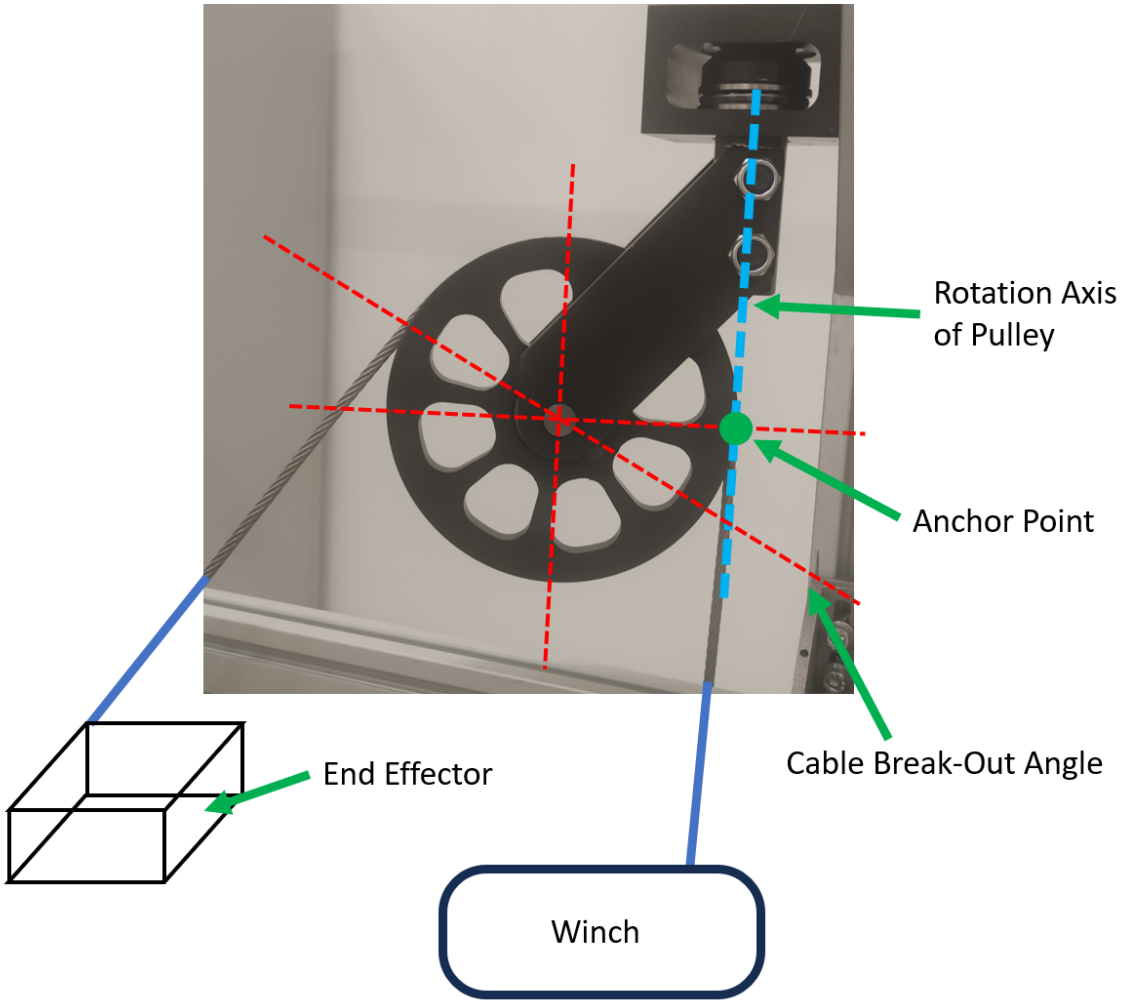

Figure 12: Working Principal of Pulleys

$$AC_{2,i} = \sqrt{{r_i}^2 - AC_{1,i}^2} \tag{7}$$

Similarly, to find the horizontal distance from the anchor point to the end-effector attachment point for the ith cable, the square of vertical height is subtracted from the square of the distance. The square root of the results gives the horizontal distance which is denoted as $AC_{2,i}$. Since the horizontal distance depends on two axes, it is easy to subtract it from the total distance, which has three axes.

$$AC_{3,i} = AC_{2,i} - Pr \tag{8}$$

Then, the horizontal distance from the pulley center to the end-effector attachment point for the ith cable which is denoted as $AC_{3,i}$. Pr is the radius of the pulley. Since the pulley is round and the cable wraps around the pulley. It would be easy to calculate cable lengths based on the pulley center.

$$AC_{4,i} = \sqrt{AC_{1,i}^2 + AC_{3,i}^2} \tag{9}$$

Where $AC_{4,i}$ is the distance from the pulley center to the end-effector attachment point for the ith cable. The magnitude of vertical and horizontal distance gives the distance from the pulley center.

$$AC_{5,i} = \sqrt{AC_{4,i}^2 - Pr^2} \tag{10}$$

Where $AC_{5,i}$ is the distance from the cable break-out point to the end-effector attachment point for the ith cable. The distance from the center of the pulley is the magnitude of the pulley radius and cable length from the break-out point to the end-effector.

$$AC_{6,i} = \arctan AC_{1,i}/AC_{3,i} \tag{11}$$

Then, the angle of the cable break-out axis is needed to be able to calculate the cable length wrapped around the pulley from the anchor point to the cable break-out point. First, the angle from the pulley center to the end-effector attachment point for the ith cable which is denoted as $AC_{6,i}$ is calculated by using the vertical and horizontal distances.

$$AC_{7,i} = \arctan Pr/AC_{5,i} \tag{12}$$

Then, the angle from the cable brake-out point to the center of the pulley for the ith cable which is denoted as $AC_{7,i}$ is calculated by using the pulley radius and the distance from the cable break-out point to the end-effector.

$$AC_{8,i} = 180 - [90 - AC_{7,i}] + [90 - AC_{6,i}] \tag{13}$$

Where $AC_{8,i}$ is the cable brake-out angle from the vertical line for the ith cable. There are three triangle vertices intersecting on the break-out axis where two of them are right triangles and the last one is the cable brake-out angle which is denoted as $AC_{8,i}$. The opposite angles of the right triangles are $AC_{7,i}$ and $AC_{6,i}$. By subtracting these angles from 90 degrees, the angles on the break-out axis can be found. By subtracting the sum of these from 180 degrees, the cable break-out angle can be found.

$$AC_{9,i} = [90 + AC_{8,i}] \cdot Pr \tag{14}$$

After finding the cable break-out point, the cable length wrapped around the pulley can be calculated which is denoted as $AC_{9,i}$. To total angle that the cable wrapped around is 90 degrees more than the cable break-out axis angle.

$$AC_{10,i} = AC_{9,i} + AC_{5,i} \tag{15}$$

Where $AC_{10,i}$ is the corrected inverse kinematic solution for the ith cable which can

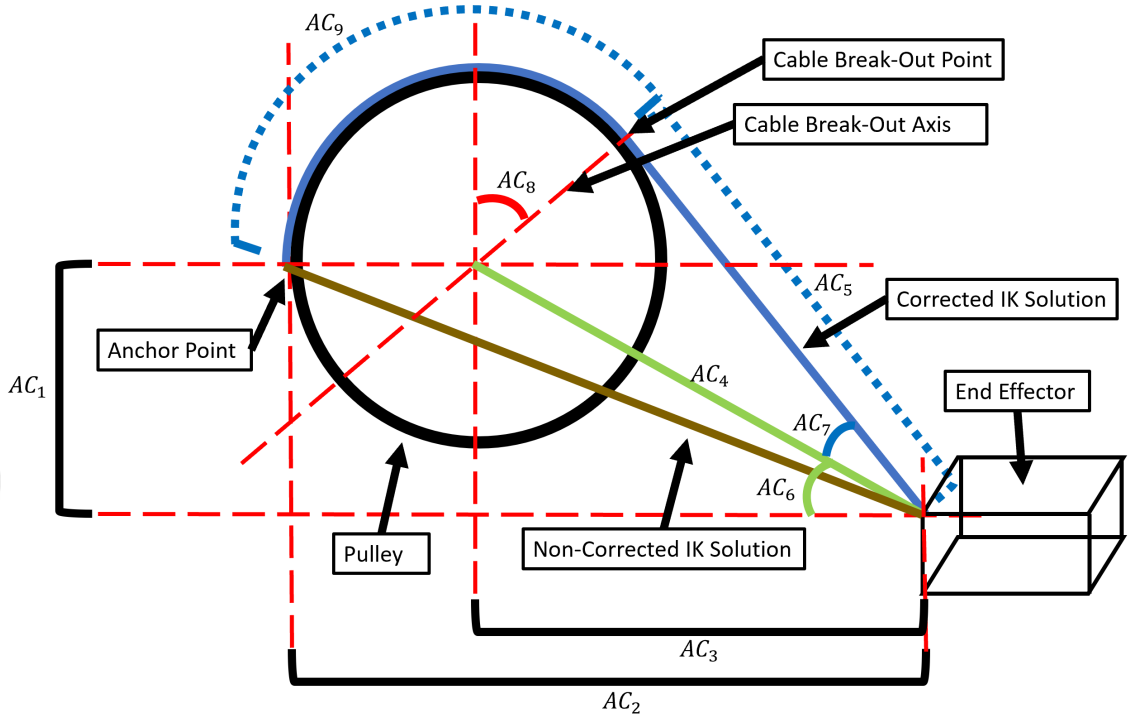

Figure 13: Anchor Point Correction Schematic View

be calculated by summing the length of cable wrapped around the pulley and cable length from the break-out point to the end-effector.

3.5 Tension Calculation

The force that causes a cable to be stretched or pulled taut is referred to as cable tension. It is a crucial idea in engineering, building, and other fields where cables are employed, including suspension systems, bridges, cranes, elevators, and even commonplace items like bicycle brake cables. A force is often applied to each end of a cable to cause it to lengthen and become taut, which, in turn, creates tension in the cable. The quantity of the applied force, as well as the characteristics of the cable, such as its length, composition, diameter, and elastic modulus, determine how much tension is in the cable.

Cable tension has a significant impact on the performance, precision, and safety of cable-driven parallel robots. Proper regulation of cable tension is vital to guarantee

the robot's stability, accuracy, and capacity to successfully complete its specified tasks.

Cable tension, which is used to optimize the design of the CDPR, is calculated for n cables. However, since there are more active cables than DOFs ($m > n$), there exist infinitely many possible solutions for a single pose of the end-effector [61]. The reuslting tension vector $\mathbf{t}$ is an $n \times 1$ vector which can be calculated using (16).

$$\mathbf{t} = \mathbf{W}^{+}\mathbf{f} \tag{16}$$

where $\mathbf{W}^{+}$ is the More-Penrose inverse of the wrench matrix and $\mathbf{f}$ is accelerations and moments on the end-effector being m$\times$1 vector. The wrench matrix $\mathbf{W}$ is defined with (17).

$$\mathbf{W} = -\mathbf{J}^{T} \tag{17}$$

where $\mathbf{J}$ is m$\times$n Jacobian matrix. However, using this derivation, some cable tension values can be found negative. Cables are non-rigid links and cannot transmit negative (compressive) force. Therefore, a lower tension limit must be set on the cable tension to have a valid solution. Likewise, cables cannot have excessive (infinite) tension, therefore, there must be a maximum cable tension limit as well. The cable tension solution must satisfy the following condition for each cable:

$$t_{min} < t_i < t_{max} \tag{18}$$

where t_{min} is the minimum allowable tension on the cables and t_{max} is maximum allowable tension on the cables. To satisfy 18, an iterative method called the dual simplex algorithm [62], which is a linear programming method to find the minimum solution, was used. In this case, minimum cable tension values are found. The dual simplex optimization in its general form is given in (19).

$$\min_{x} c^T x \text{ such that } \begin{cases} Ax = b \\ lb \leq x \leq ub \end{cases} \tag{19}$$

where $A \in \mathbb{R}^{m \times n}$, lb is lower bound of the solution and ub is upper bound of the solution.

3.6 End-effector Compliance Index (ECI)

In order to determine the optimum size of a CDPR, a series of simulations were run and the results were analyzed. In literature, cable-based robot designs are optimized using a set of performance indices, such as manipulability, power dissipation, and dexterity [63]. In [64], a method for determining the motion of the cable anchor points using the dexterity index and elastic stiffness index to ensure optimum dexterity with the best practical elastic stiffness was introduced for planar adaptive cable-driven parallel robots. However, there was not enough research on finding optimum anchor point locations of a redundant CDPR. Therefore, in this work, cable tension values and end-effector stiffness of a redundantly actuated CDPR were studied. To evaluate the stiffness and cable tension values, an index was created so that the stiffness could be quantified. For simplicity and a better understanding of the design parameters, the reciprocal of the stiffness, that is compliance, is quantified with a new index and defined as the *End-effector Compliance Index (ECI)*. The index is calculated for different poses of the end-effector and for different anchor point locations on the frame. The index is purely a geometrical property of a single pose of an end-effector for the configured anchor points. The flexure of the physical robot is not included in ECI calculations as all physical components of the CDPR are assumed to be rigid for simplification. The ECI uses the unit vectors defining the direction of cables (20) and cable lengths (4).

$$\hat{\mathbf{u}}_i = \frac{\mathbf{d}_i}{r_i} \tag{20}$$

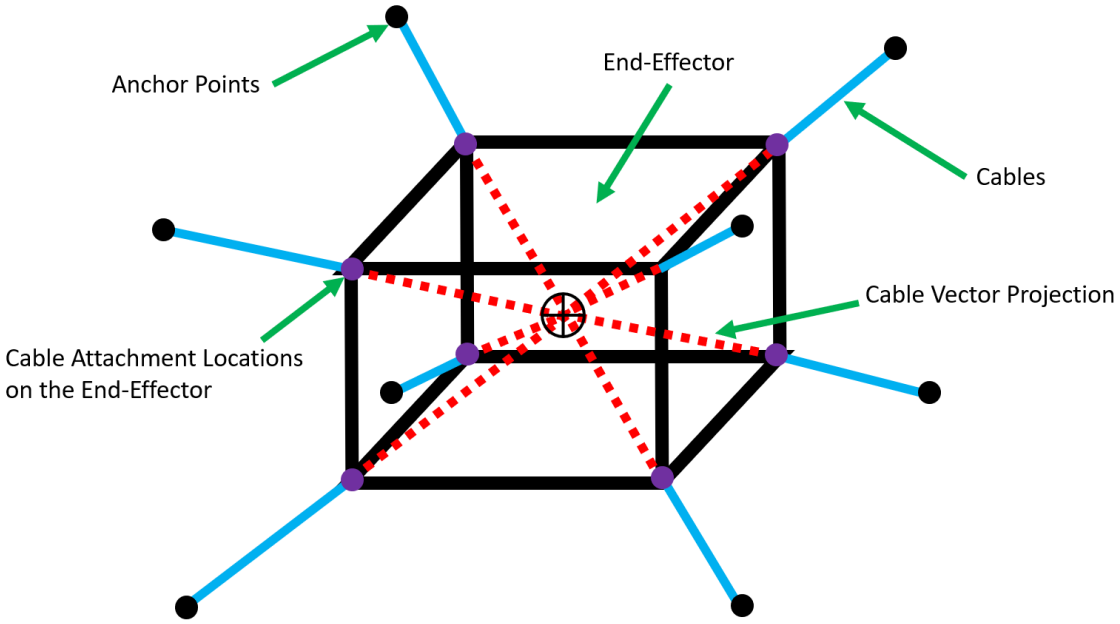

Figure 14: Zero ECI Schematic View

The unit vectors, $\hat{\mathbf{u}}_i$, are scaled by the mean of all cable lengths, $\overline{r}$. The magnitude of the vector summation determines the ECI as in (21).

$$ECI = \|\sum_{i=1}^{n} \hat{\mathbf{u}}_i \overline{r}\| \tag{21}$$

The ECI would be zero when the unit vectors of all the cables are perfectly opposed to each other and the end-effector would be in the stiff (or the least compliant) configuration. Such configuration can be seen in Figure 14. If the ECI has a positive value this would show that the end-effector would have lower stiffness since the unit vectors of the cables have variance among them. The ECI would be maximum when non of the cable's unit vectors intersect at any point in the space. In this configuration, the end-effector is the least stiff (or the most compliant) configuration. Such a configuration can be hanging the end-effector from the ceiling with parallel cables which can be seen in Figure 15. In such a configuration, any disturbance will greatly affect the pose of the end-effector.

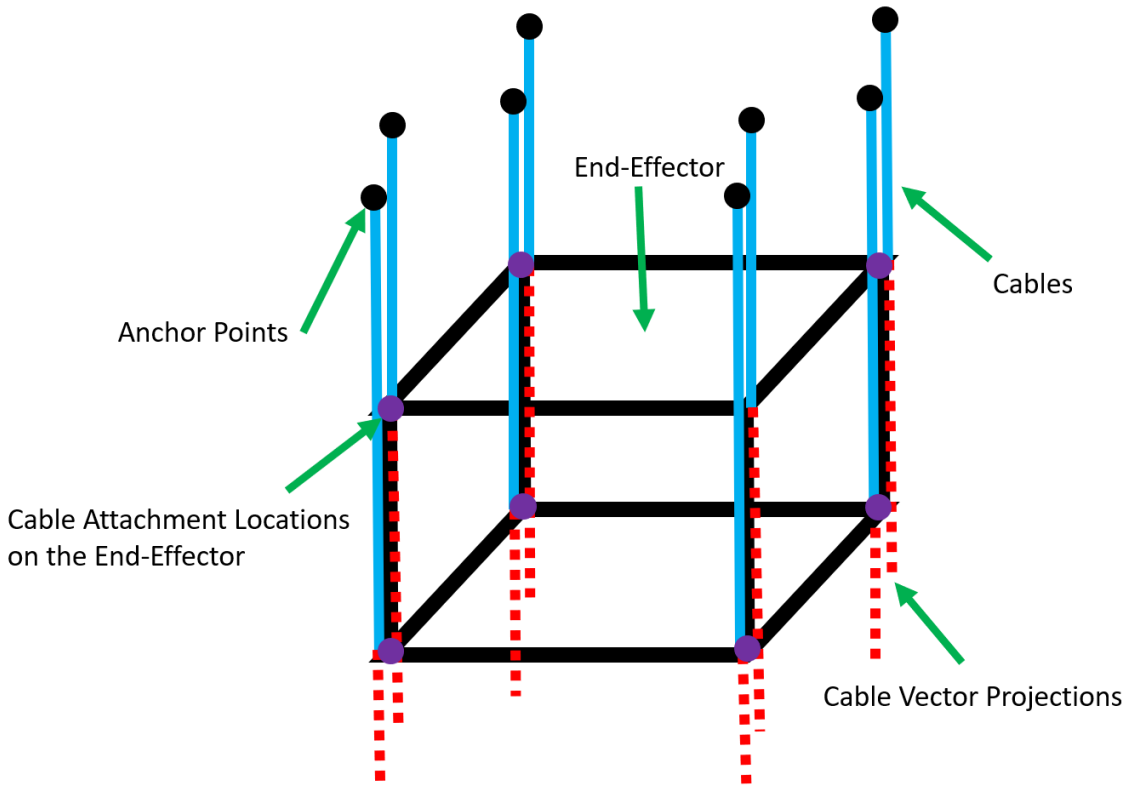

Figure 15: Maximum ECI Schematic View

CHAPTER IV

ANCHOR POINT SELECTION METHODOLOGY

In this chapter, the methodology used to select cable anchor points of a CDPR is explained to design better-performing CDPRs. The methodology uses a new index called End-Effector Compliance Index. End-Effector Compliance Index is compared with mean cable tensions. The comparison uses different anchor points and different print parts to find a relation between the stiffness of the end-effector and the built cost of the robot. According to the obtained relation, cable anchor points can be selected. Also, to limit the scope of the study, only print paths for half-cubes are examined, and cable anchor points are placed on the vertical edges of the CDPR. The frame of the CDPR is a half-cube to maintain symmetry on the anchor points. The end-effector used in this work is also a half-cube with a 0.2m base size length and 0.1m height. The weight of the end-effector is set to be 25 kg.

In additive manufacturing, complex objects could be created by adding layers of material one at a time. Very complex shapes can be produced with the technology. In this study, half-dimension cubes are used to represent complex additive manufacturing parts. The dimensions of these half-cubes are acceptable in size similar to the complex-shaped pieces that can be printed.

The variation of ECIs and mean cable tensions depending on the dimensions of the CDPRs was examined. Cable anchor points were positioned on the vertical edges of the frame and upper anchor points were placed at the top vertices. To create a constrained CDPR, lower anchor points were placed at the height of the printed half cube. If the lower anchor points were to be placed lower than the height of the printed part, either the cables or the end-effector might hit the printed part. Also, to

create a suspended CDPR, lower anchor points were placed above the end-effector. An example suspended CDPR frame with 1.0m square base and 0.5 height, and a print part with a 0.4m square base and 0.2m height are shown in Figure 8.

Simulations were conducted for printed parts with base edge lengths ranging from 0.2m to 0.8m in 0.2m increments. Figure 16 shows the ECI and mean tension variation of the constrained and suspended type CDPRs together for a printed half-cube that is $0.2 \times 0.2 \times 0.1$ m in size. Constrained CDPRs have lower ECI values than suspended CDPRs. On the other hand, constrained CDPRs have higher tension values than suspended CDPRs. With increasing the dimension of a CDPR, ECI increases while mean tension values decrease.

Separate simulation result plots for constrained and suspended CDPRs can be seen in Figures 17 and 18, respectively. Also, by placing 4 different print part results into a graph, a trend line can be seen. With increasing the dimension of a CDPR, ECI increases. On the other hand, with increasing the dimension of a CDPR, the required cable tension value decreases. For constrained CDPRs, the ECI is almost lying on a line with minimal change for different print part sizes. For a suspended robot, the ECI shifts to the right with increasing print part sizes meaning that the same ECI value can be achieved for a bigger print part with a bigger CDPR. Also, increasing print part size increases the required tension value for both suspended and constrained CDPRs.

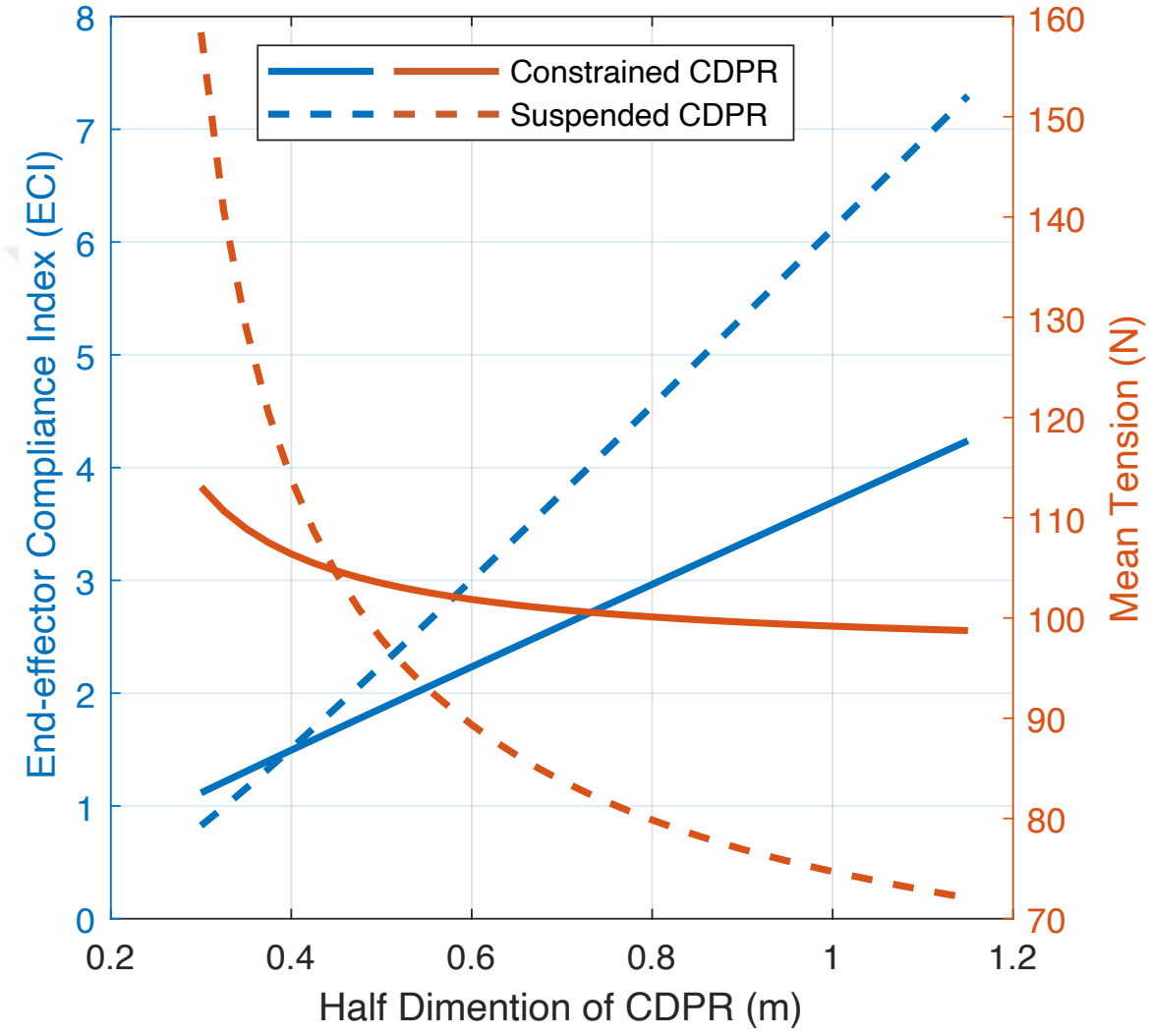

Figure 16: Plots show the ECI (blue lines) and mean tension (orange lines) vs half dimension of CDPR for a printed half-cube with a 0.2m square base. The solid lines show the constrained CDPR configuration and the dashed lines show the suspended CDPR configuration.

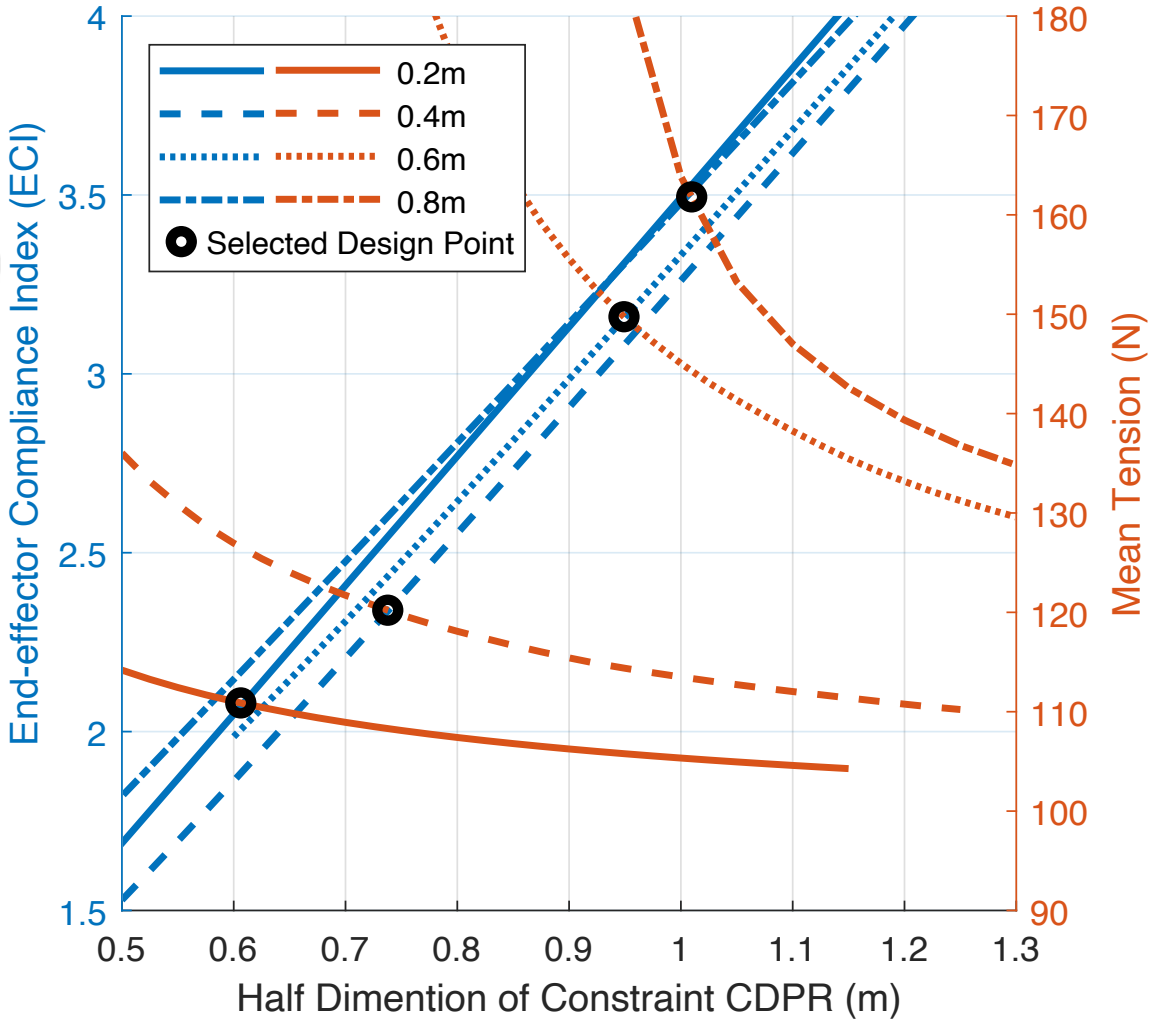

Figure 17: Plots compare ECI and mean tension depending on the half dimension of constrained CDPR for different-sized print parts. Line types represent different half-cube print sizes. The optimum CDPR dimension is selected as the point where the ECIs cross the mean tension values and shown with black circles. The solid black line is the best fit for the selected optimum CDPR dimensions.

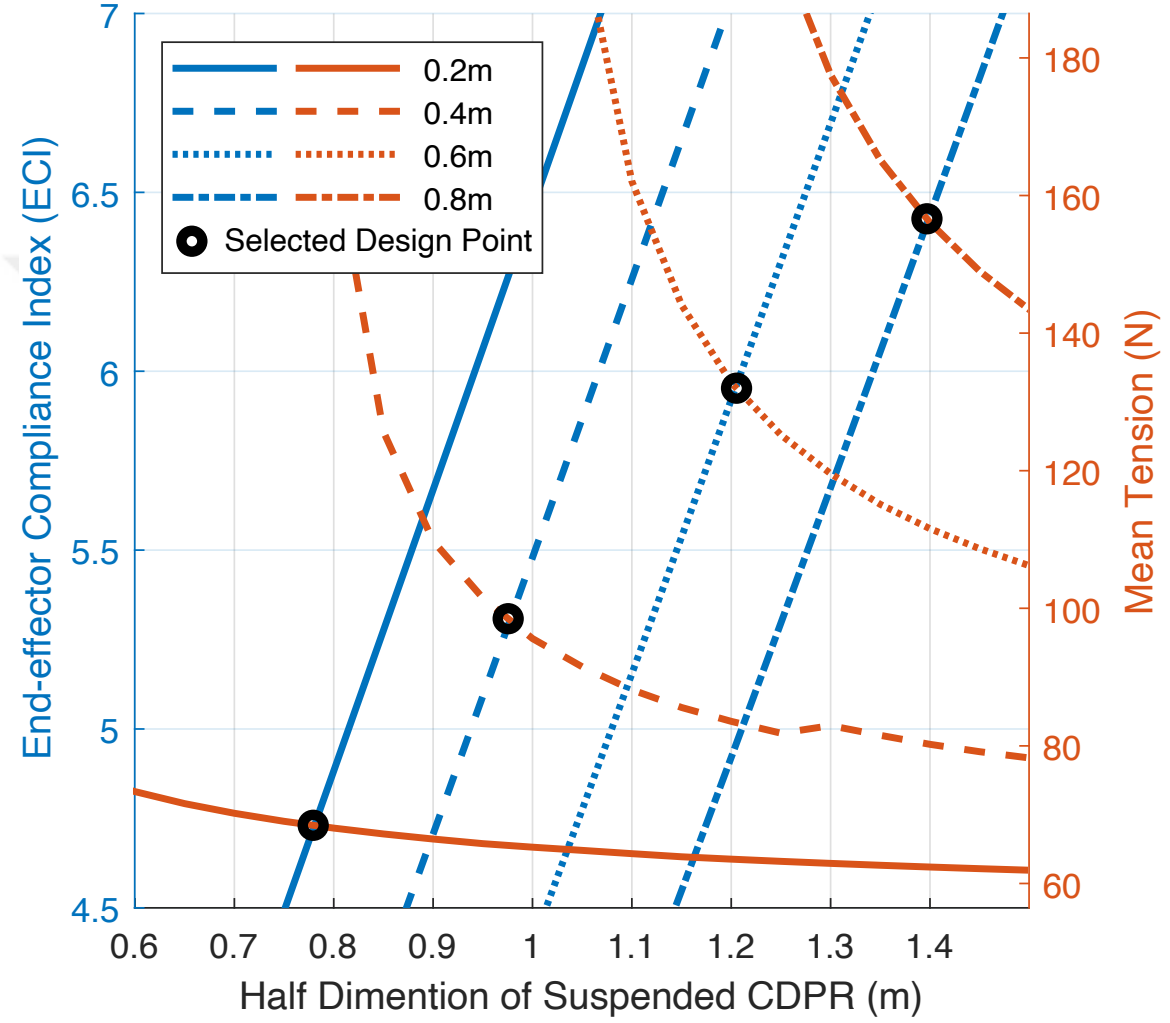

Figure 18: Plots compare ECI and mean tension depending on the half dimension of suspended CDPR for different-sized print parts. Line types represent different half-cube print sizes. The optimum CDPR dimension is selected as the point where the ECIs cross the mean tension values and shown with black circles. The solid black line is the best fit for the selected optimum CDPR dimensions.

CHAPTER V

RESULT OF SIMULATIONS

Based on the simulation results, to have a lower ECI value, the CDPR dimensions should be kept at a minimum and to have lower cable tension, the CDPR dimensions should be higher. Also, constrained CDPRs generally have a lower ECI, and suspended CDPRs generally have less cable tension values (as seen in Figure(16)). However, because cable tension is compared with the ECI, suspended CDPRs have higher tension values than constrained CDPRs to have a relatively low ECI. If suspended CDPRs are allowed to have much higher ECI values, the mean cable tension would be less than constrained CDPRs. However, this increases ECI and reduces the stiffness of the end-effector.

CDPR dimension is directly correlated to print part size regardless of constrained or suspended type. The size of a CDPR should be determined according to the size of the print part. Simulation is conducted for 4 different half-cube print part sizes for base edge lengths of 0.2m, 0.4m, 0.6m, and 0.8m. Optimum CDPR dimension sizes are chosen as the values where ECIs cross mean cable tension values since the crossing points yield the best possible result combination for both ESI and mean cable tension. If any other point would be selected, either ECI or mean cable tension would have a less desired value in order to have a better value for the other parameter. For suspended CDPRs, the optimum half dimensions of bases are 0.78m, 0.98m, 1.21m, and 1.40m respectively. For constrained CDPRs, the optimum half lengths of bases are 0.61m, 0.74m, 0.95m, and 1.01m respectively. To have less cable tension, these base dimensions can be increased and to have a stiffer end-effector, these base dimensions can be decreased.

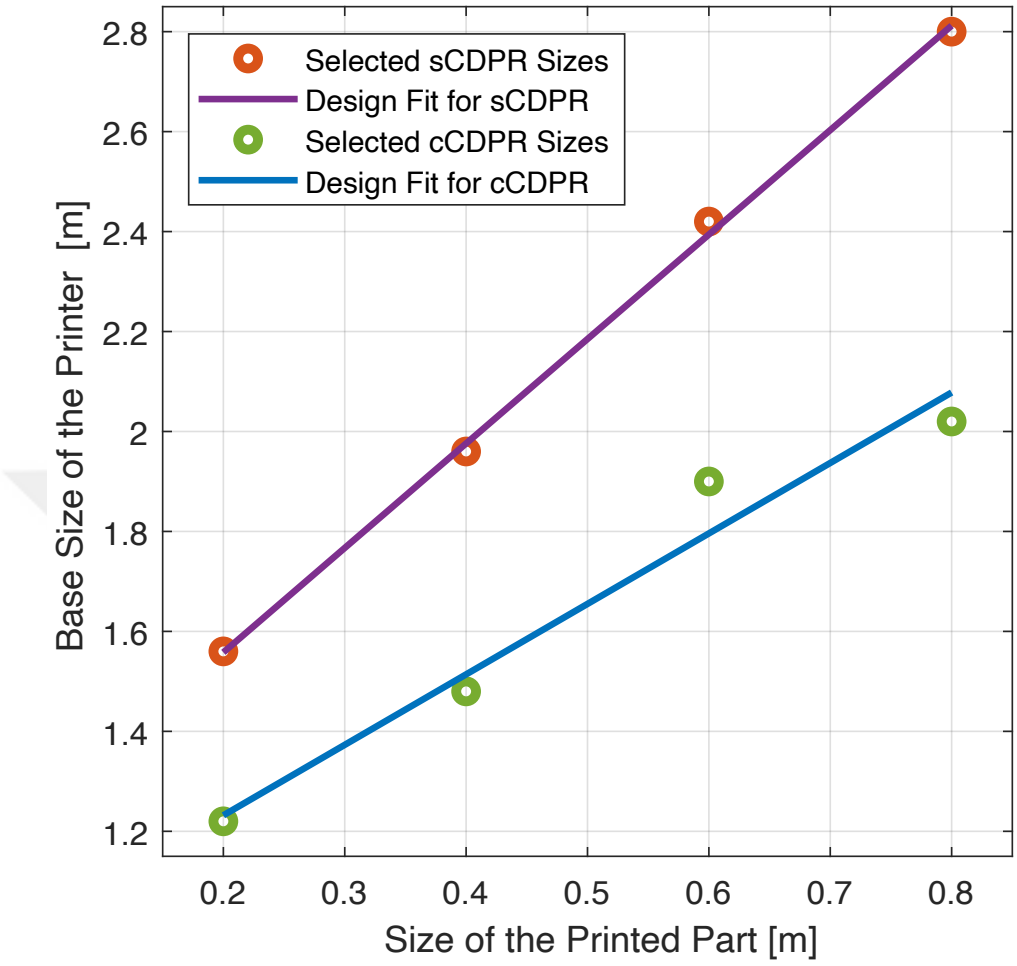

Figure 19: Circles show optimum CDPR base sizes for desired print parts. The purple line is the best fit for optimum suspended CDPR and the green line is the best fit for optimum constrained CDPR base sizes.

The optimum CDPR points chosen seem to lie on a straight line (see Figure 19). If the best linear fits were chosen for these points, the coefficient of determination (R^2) would be 0.9625 for constrained CDPR and 0.9823 for the suspended CDPRs. The line equations are given in (22) and (23) for suspended and constrained type, respectively.

$$s = 2.09a + 1.14 \quad [m] \tag{22}$$

$$s = 1.41a + 0.95 \quad [m] \tag{23}$$

where a is the size of any print part and s is the corresponding dimension of the CDPR. Using these fits, the optimal CDPR dimension can be found for any print part. The coefficients of determination values of the fits, which are close to 1, show that the selected sizes would be optimal.

Another observation from Figure 17 is that the ECI lines seem to coincide for constrained CDPR designs. The reason for this is that the CDPR dimensions and printed part dimensions scale similarly. Because with the size change, lower pulleys would always be placed at the height of the print part, and the distance between the upper and lower pulleys will scale according to CDPR dimension. On the other hand in Figure 18, for suspended type CDPRs, the distance between lower and upper pulleys is always constant and does not change with CDPR dimension change. Therefore, the ECI curves shift laterally with size increase. Having a higher distance between the lower and upper pulleys shifts the ECI curve toward the right. This also changes the place where the ECI crosses the mean tension values, making the optimum CDPR dimension larger and the mean of the cable tension value lower.

CHAPTER VI

IMPLEMENTATION OF CDPR DESIGN METHODOLOGY

The following chapter introduces the implementation of the presented methodology. The methodology has been applied to a case study. The design and construction of the robot in the case study have been explained.

6.1 Case Study

A suspended CDPR for additive manufacturing operations was designed. The desired print part base length was 1m. According to the equation 22, the selected base length of the CDPR should be 3.23m. The ECI was almost 7, and the mean cable tension value was 185N. However, to have better print results, the stiffness of the end-effector was decided to increase. This decision requires reducing the size of the frame and increasing the mean tension value. The frame dimensions were reduced to 3/4 of what equation 22 suggests which was 2.4m. The reduction in the frame size lowers the ECI to 4.13 and increases the mean cable tension to 352 N. Reduction in ECI increases the stiffness of the end-effector and the print quality. On the other hand, the robot requires powerful motors and a stronger structure to withstand the increased cable tension values.

6.2 Design and Construction of the CDPR

In this section, part of the CDPR has been explained which are a frame, cables, pulleys, winches, an end effector, and an electrical panel.

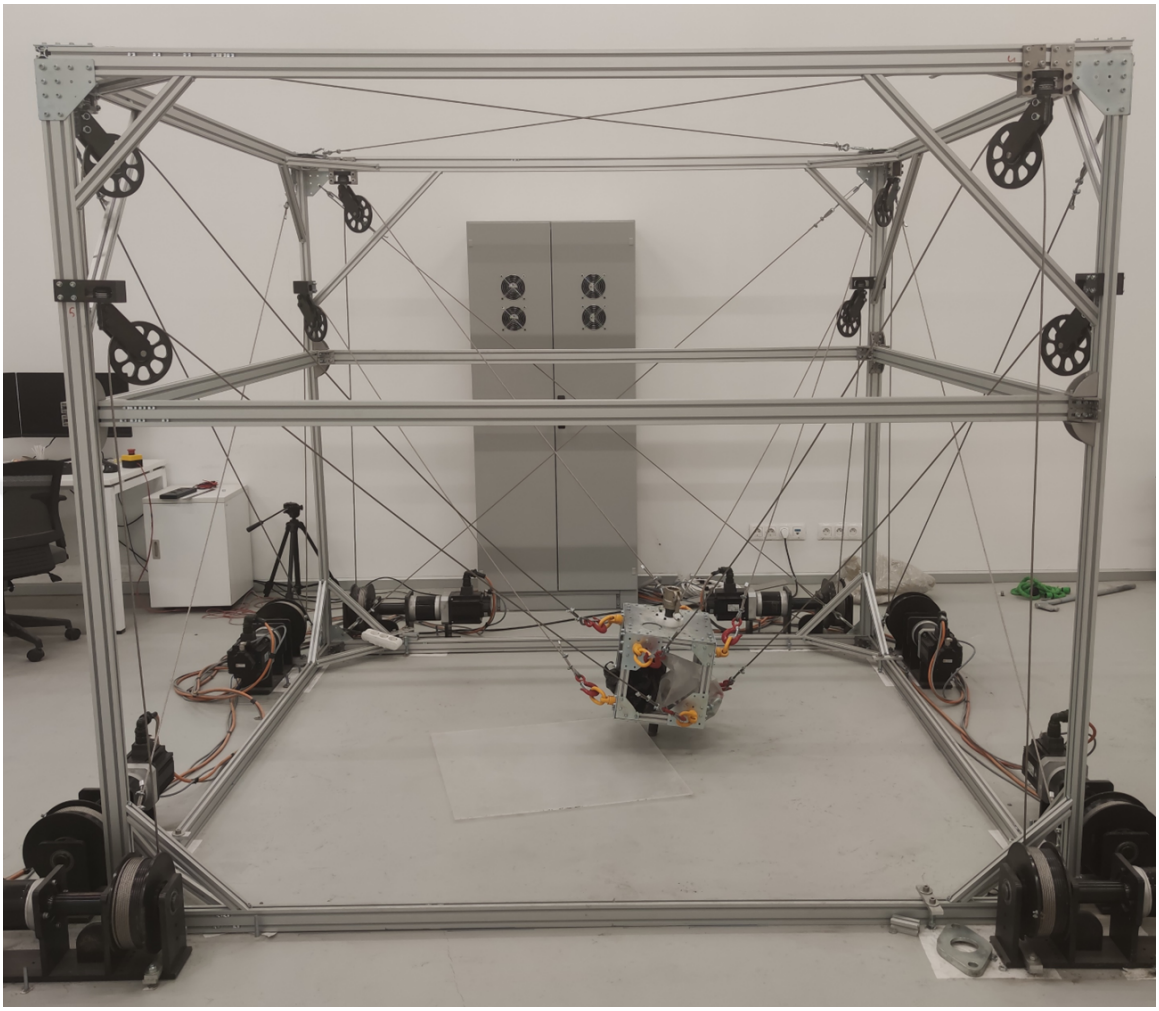

Figure 20: Constructed CDPR Frame

6.2.1 Robot Frame

The frame of a cable-driven parallel robot (CDPR) is the stiff framework that gives the robot its overall form and stability. It serves as the foundation for placing the other parts and constitutes the robot's backbone. The frame of a CDPR is frequently made up of multiple connected stiff parts or beams. Materials like aluminum, steel, or carbon fiber may be used to create the frame due to their strength, stiffness, and lightweight qualities. The precise design of the frame may change depending on the robot's intended use, size, and cargo capacity.

The frame of the CDPR is made of aluminum strut profiles having a cross-sectional

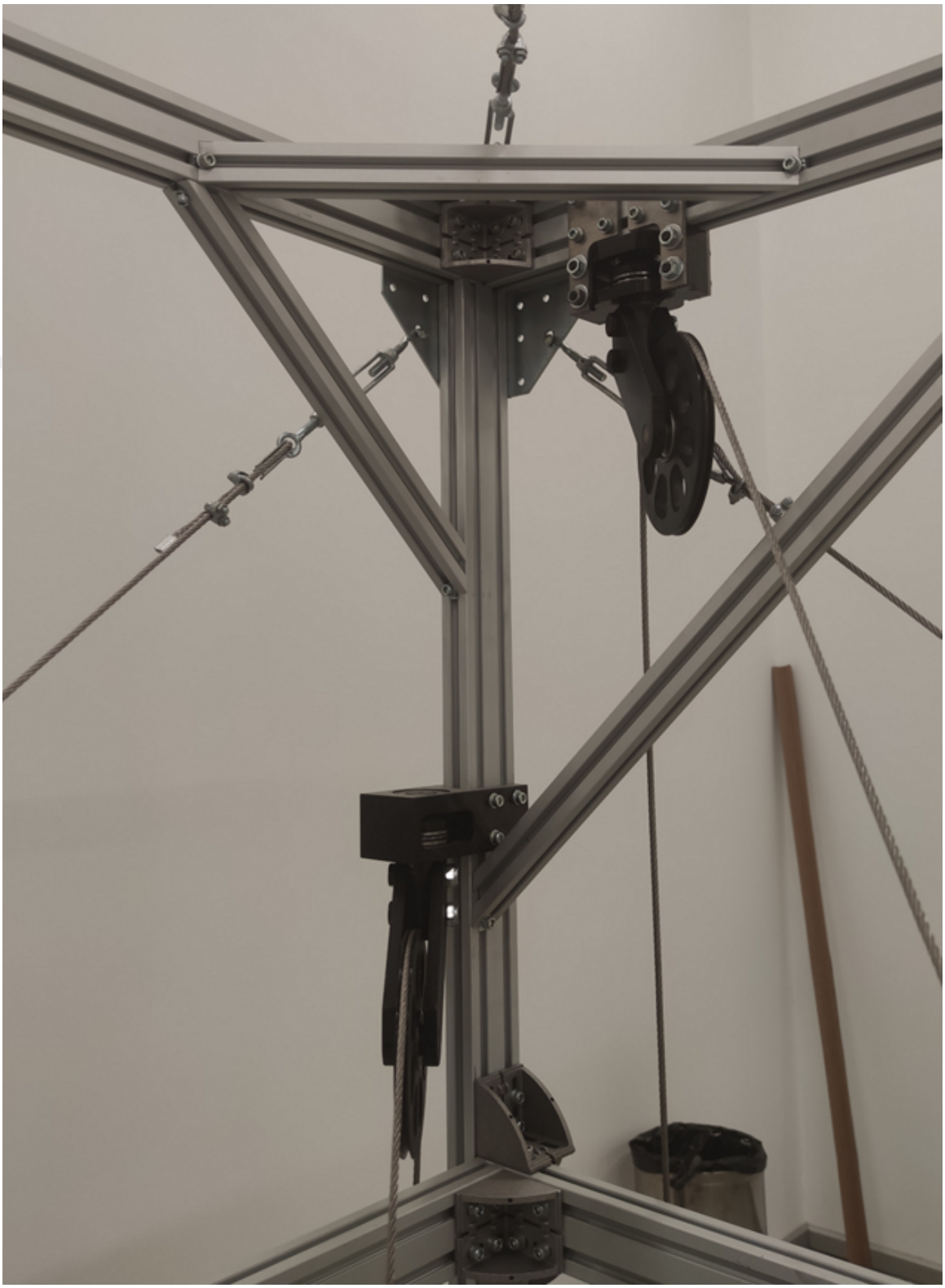

Figure 21: Upper and Lower pulleys and Single Corner of the Frame

dimension of 30 x 60 mm. The size of the frame is 2.4 x 2.4 x 2.0 m and has a height of 2.0 m. The corners are supported with laser cut plates, special braces for strut profiles, and a cross-sectional dimension of 30 x 30 mm strut profiles to increase the stability of the frame. A single corner of the frame is shown in Figure 21. To further reduce the bending of the frame, corner-to-corner tensioners are used to preload the frame diagonally. Hence, the forces causing the frame to bend will be carried by the tensioners and do not have a significant effect on the frame. This increases the stability of the frame consequently enhancing the precision of the end effector. The frame is also bolted to the ground to reduce any movement of the frame relative to the ground adding to the aforesaid. The machined frame is shown in Figure 20.

6.2.2 Stainless-Steel Cables

Cables made of stainless steel, a type of steel alloy with at least 10.5% chromium, are known as stainless steel cables. The distinctive qualities of stainless steel, such as corrosion resistance, high strength, and durability, result from the addition of chromium to the steel composition. Due to these qualities, stainless steel cables are ideal for a variety of applications, particularly those that require them to operate in challenging situations where normal steel cables may corrode or degrade over time.

The cables should be strong enough to carry the required tension values safely. Cables have their load capacities as well as minimum bending radius [65]. In other words, with the increasing diameter of cable cross-section, their allowable load increases, as well as their minimum bending radius. The cable selected for the robot was a 7x19 independent wire rope core (IWRC) stainless steel cable which can be seen in Fig 22. The minimum bending radius of the cable is 12 times the diameter of the cable. Since the diameter of the cable is 5 mm, the minimum bending radius is 60 mm. Also, the selected cable has a minimum breaking load of over 1200 kg, moderate flexibility, and resistance to corrosion. The failure criteria of these cables

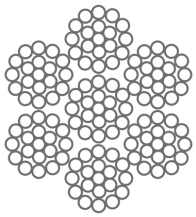

Figure 22: Cross section of the 7x19 IWRC cable

for this project is to exceed their yielding points. Cables are rated to their breaking loads and this is well beyond their yielding points. For example, austenitic stainless steel has a yielding point of around 250 MPa and maximum tensile Stress of around 600 MPa [66]. Therefore, the cable used in this project may fail around 500kg load. In this project, the estimated maximum load on the cables is 3kN which is in the elastic deformation region of the cable.

6.2.3 Pulleys

A pulley is a straightforward device that consists of a wheel with a groove positioned on an axle or shaft. It can be used to raise items, transmit power, or change the direction of a force. The rope or cable that passes through the pulley's groove is referred to as a "belt" or "cable." Pulleys are frequently employed in a variety of applications to facilitate work by lowering the force necessary to move large objects or raise loads. They are extensively employed in businesses, building projects, transportation, and everyday objects.

A total of 8 pulleys are used in the robot, two on each corner frame. Pulleys re-direct cables from winches to the end effector and can rotate on the vertical axis. When the end effector moves to another position, pulleys passively change angles and follow the required angle of the cables for the new position of end effector. The vertical rotation axis of the pulley is tangent to the pulley disc, making it not affect the pulley angles at the cable release points. This factor also plays a vital role in cable winding on drums. Since there is no active cable guide for winding and unwinding

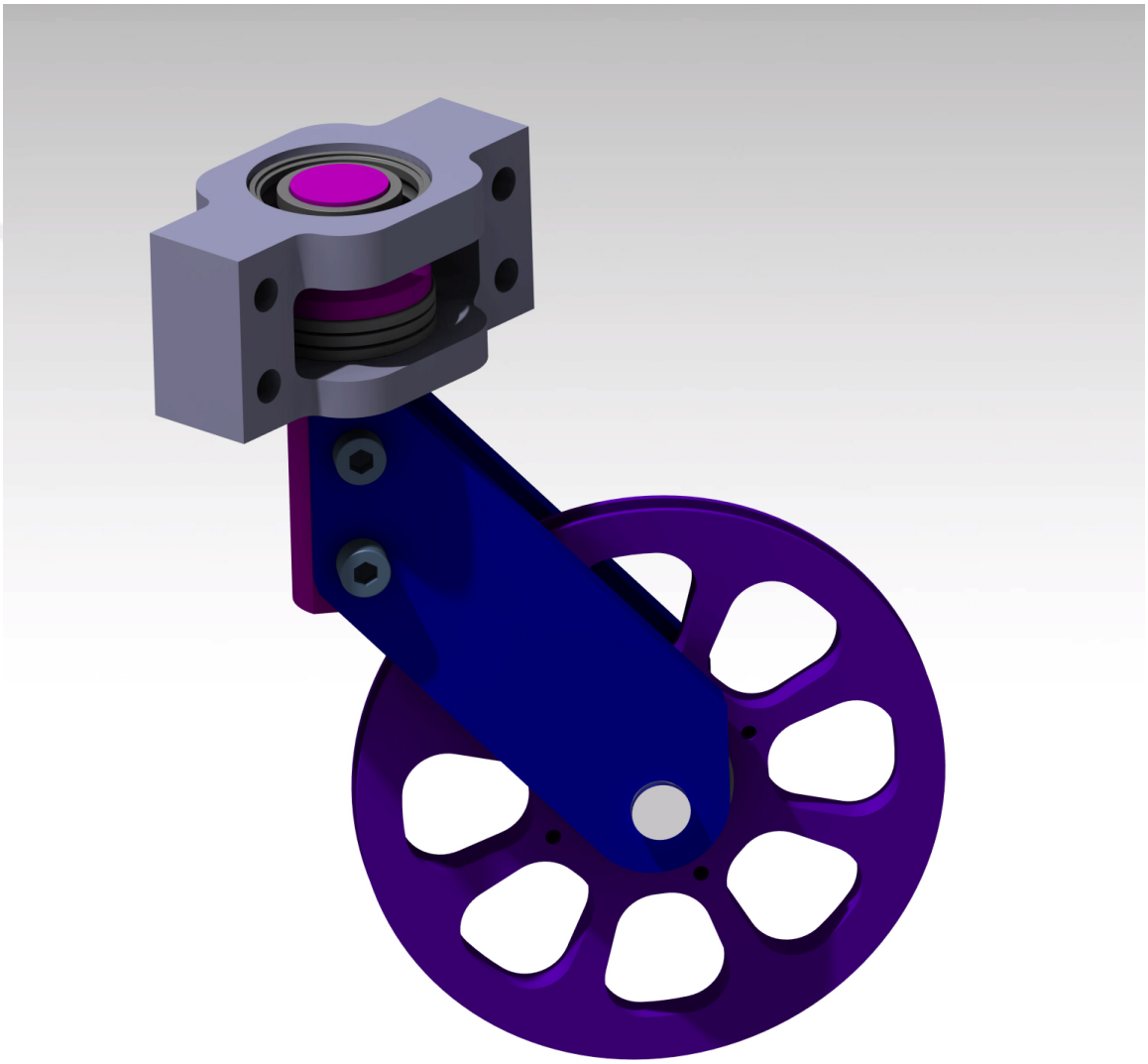

Figure 23: Design of pulleys.

Figure 24: Machined pulley

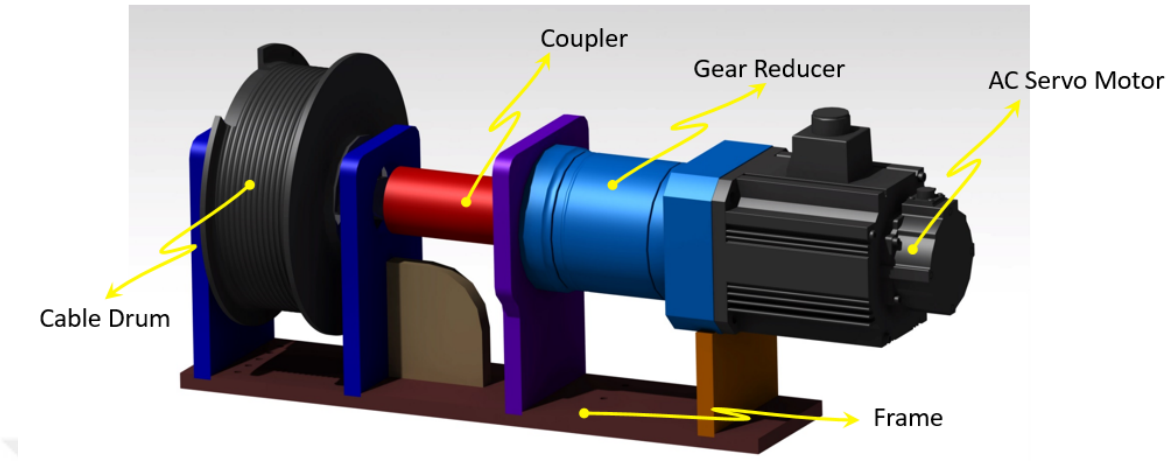

Figure 25: Design of winches.

on the drums, the approach angles of cables should be between 0.5 to 2.0 degrees. Moreover, the vertical rotation axis of pulleys tangent to the pulleys allows no angle change of cables for different end effector positions. The Pulley assembly used is shown in Figure 23. The machined pulley is shown in Figure 24.

6.2.4 Winch

A drum or spool around which a cable or rope is wound makes up a winch, a mechanical device. It is used to transfer loads horizontally, raise or pull big objects, and carry out other operations that require precise control over a strong pulling or lifting force. Depending on the use and the required pulling force, winches may be hydraulically, electrically, or manually operated. They are built with safety elements to guard against overloading and to provide smooth and regulated operation. They are designed with varying load capacities to fit different tasks. In addition, the term "winch" can refer to the entire winching system, which includes the cable or rope, the spool, the engine or power source, and any related control devices.

The winches are placed on the ground below each pulley. Winches are assemblies of different components which are the motor, gearbox, coupling, drum, and frame. The motor used is an AC servo motor having 1.5 kW power which can give 7.16 Nm

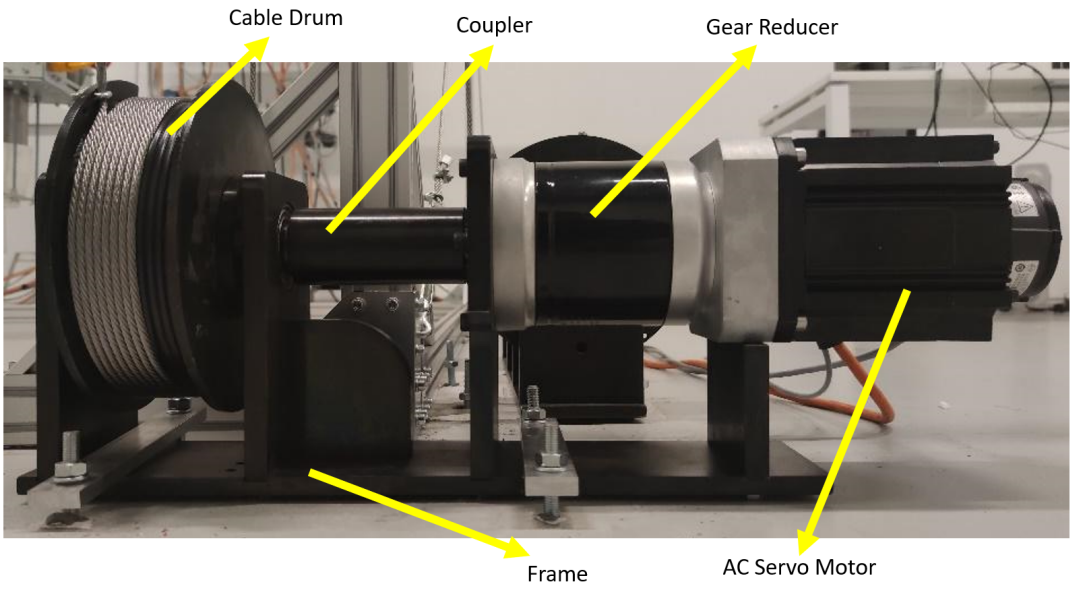

Figure 26: Machined winch

torque output from 0 to 2000 rpm. The gearbox ratio is 1/50 which makes the torque output of the gearbox 333 Nm with frictional losses and makes the rotational speed output 40 rpm. The coupling which connects the gearbox to the drum is made of a solid cylinder to minimize any backlash between the gearbox shaft and the drum shaft. Since the position of the drum is essential for the position of the end effector, any flex on the coupling reduces the precision of the end effector. The drum has cable grooves to guide cable winding and unwinding evenly. Since there is no active cable guide on the drum, grooves are needed to increase the maximum allowable cable approach angle on the drum. All the parts are supported by the frame and the frame is bolted to the ground below each pulley. The winch assembly used is shown in Fig. 25. The machined winch is shown in Fig. 26.

6.2.5 End-Effector

A tool or device attached to the end of a manipulator or robotic arm is known as an end effector. It is the component of the robot that interacts with the outside world to carry out a certain mission or function. The end effector is in charge of performing

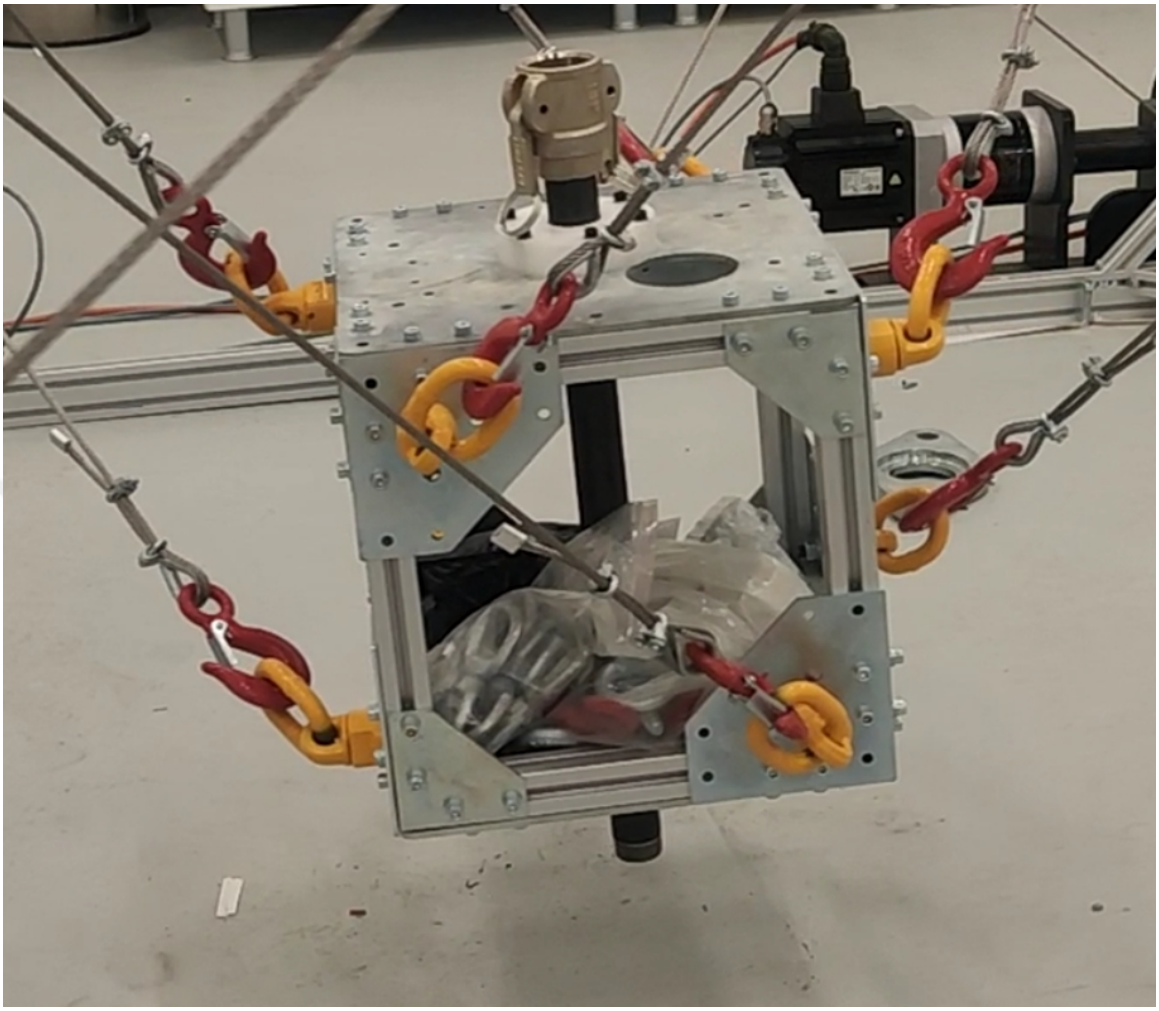

Figure 27: Machined cubic-shaped end-effector for 8-Cable, redundantly actuated, suspended CDPR for additive manufacturing.

the intended action or operation as instructed by the robot's control system. The choice of end effector depends on the application and the task that the robot is supposed to perform. Robots can be flexible and adaptive in numerous industries due to several types of end effectors that can be built and adapted to suit different tasks. End effectors are essential to the overall effectiveness and usefulness of robotic systems. They enable robots to perform a variety of tasks, including assembling goods, packaging, handling materials, inspecting, and much more.

The end effector frame is a cube of 30 cm edge length and made of strut profiles. Cables are attached at each corner of the cube frame with swivel eye bolts. Swivel

eye bolts are placed at the side of their placed corners to increase the flexibility of the end effector. The tank, nozzle, and motor assembly are bolted onto the cube frame. In this way, there is no external stress on the printing assembly due to the high tension on the cables. The end-effector is shown in Figure 27.

6.2.6 Electrical Panel

An electrical panel functions as a hub for delivering electricity to numerous machines, appliances, and equipment. Electrical panels are essential for the safe and efficient organization and distribution of electrical power. They make it easy to upgrade, maintain, and troubleshoot electrical systems. Depending on the specific usage and requirements, electrical panels can be small residential distribution boards or large industrial control panels used in manufacturing facilities or power distribution centers.

An electrical panel is used to contain electrical equipment for the robot. The panel creates a safe environment by separating the electrical parts from the rest of the system and the environment. The panel dimensions used in this project are 800x1800x500 mm. This dimension is enough to contain all the necessary equipment for the robots which are a workstation, a motion card, 8 servo drivers, 2 terminal boards, 8 magnetic contactors, 2 power supplies, 4 cooling fans, and necessary circuit breakers. The electrical panel can be seen in Figure 28.

The workstation does all the required calculations for the robot's motion and contains all the coding inside. The motion card for the servo drivers is also attached to the workstation. The motion card model is from ADLINK with the model number PCI-8258. This PCI card is capable of running 8 servo motors at a time with the servo update rate 20kHz. The servo card is connected to the servo drivers via 2 terminal boards with model number DIN-825-GP4. Each of these terminal boards is attached to 4 different servo controllers and has 100 additional pins to be able to exchange analog and digital signals.

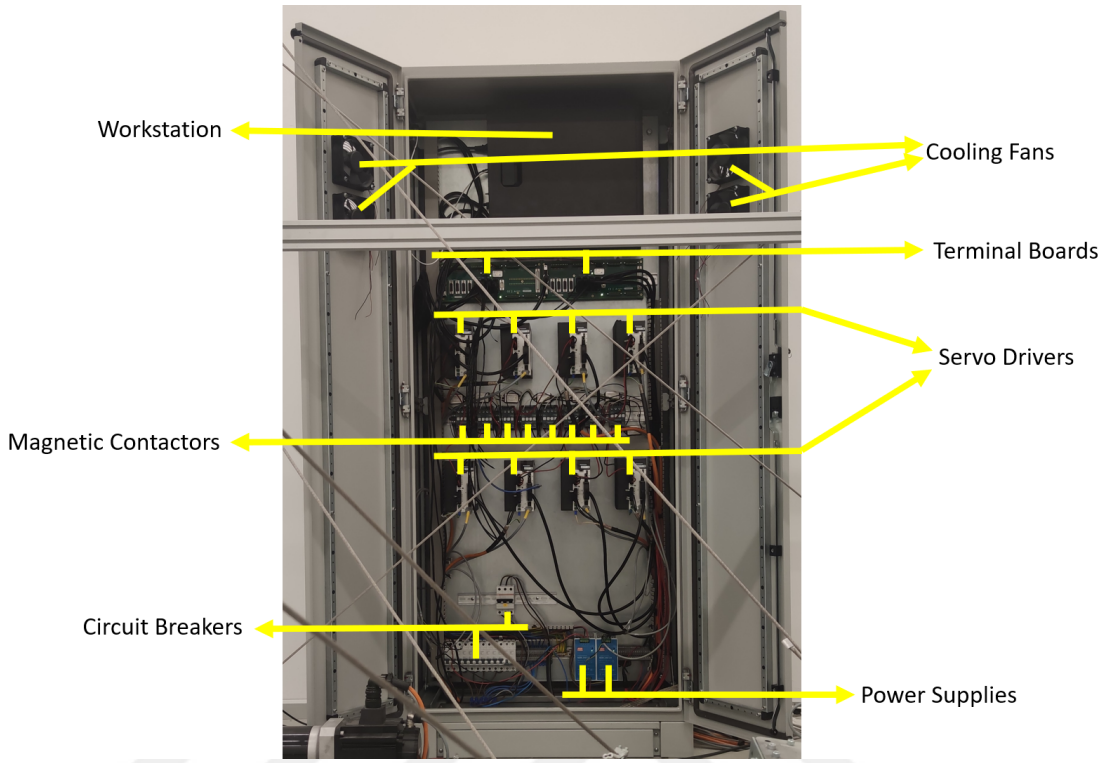

Figure 28: Electrical Panel of the CDPR

For each servo motor, there is a servo driver. The servo drivers are capable of outputting 1.5 kW of power from Panasonic with the model Minas A5. Between the servo drivers and the circuit breakers, there are magnetic contactors. These magnetic contactors are wired to a safety switch to cut the power of the drivers in an emergency. This method is actually not favorable since cutting the power of servo drivers directly might damage them. There are emergency pins on the terminal board for each servo driver to be programmed and used in an emergency.

Lastly, power supplies are 24 V and used for powering the terminal boards, cooling fans, and brakes of the servo motors. For each motor driver, there is a circuit breaker. There are circuit breakers for the workstation and the power supplies.

6.3 Control of CDPR

The following chapter explains the software part of the CDPR controls. Each motor's parameter was set in PANATERM software. Then, their motion control cart's

parameters were set in Motion Creator Pro 2 and run together to be sure that the motors work. Then the necessary codes were written in MATLAB.

6.3.1 Parameters of Servo Drivers

In this study, industrial AC servo drivers and motors were used. Servos were set to rotate a single revolution for every 1000 pulses. This makes the resolution of the pulses 0.36 degrees. Also, there were 1 to 50 gear reductions on the servo motors. Therefore, the resolution after the gear reduction was 0.0072 degrees. The gear reduction was attached to a drum that has a 10 cm radius. The linear resolution of the cables was 0.13 nm.

The motors were controlled by a motion card. The motion card can run 8 motors at a time and has a servo update rate of 20 kHz. Motor parameters were set to the motion card such as encoder resolution and rotation direction.

6.3.2 Motion Control

In general, Visual Studio was used to write the necessary codes for industrial servo motors. However, coding a system in MATLAB is favorable due to the ease of getting sensor data. Motion card has a complete library to do various thing which is called API. To use the motion card's built-in commands, the library was imported into MATLAB. Then, the APIs were written as MATLAB functions to make use of them easier.

6.3.2.1 Homing of Cables

The servo motors have incremental encoders. This means that the encoder value will be lost after power-down the servo drivers. Servo motors lose their position when they were powered down. When servo drivers were powered on, the position values were basically meaningless. This required a homing sequence after the power-up of serve drivers. For homing the servo motors, there was no limit switch on the cables.

The homing was done by controlling the cable length of each joint. The hook which was attached to the end of each cable needed to be placed 30 cm below the horizontal line of the corresponding pulleys. The distance was measured with a ruler. The cable length was adjusted on the software manually until the distance was correct. The encoder value for a 30 cm cable length was known and set to the corresponding servo motor. The length was calculated by adding the distance of half circumference of the pulley and 30cm of cable length. The corresponding length was converted to the pulse number. The pulse number was then set to the motors. Then, the motors know their positions. This homing sequence was done one by one for each motor. After homing a servo motor, the hoke was sent to the home position of the motor and attached to the end effector. After homing all the motors, the end effector will be at the home position.

6.3.2.2 Motion Command

There were many command lines for the servo motors. The control card has a built-in library to be able to control every parameter or aspect of the servo motors. In this library, there were many motion types to choose from according to the users' needs. Because there were 8 joints, 8 motors needed to be controlled at the same time to be able to control the position of the end effector. There were a few motion commands to do that. The one that allows controlling of all the aspects of the motion is called "APS_line_all". This motion code starts all the joints at the same time and finishes the motion of all the joints at the same time. This means that, regardless of the distance difference between the joints, all the joints will start and finish at the same time. The joint motions were linear. "APS_line_all" also requires end velocity, max velocity, start velocity, acceleration, and deceleration of the motion. There was also another parameter called "Sfactor" which determines the interpolation rate of the current motion with the forthcoming motion. This parameter links sequential motions

together. To move the end effector, the motion should be divided into smaller motions and sent in an order. These serial motion commands needed to be linked together to eliminate the vibration of the end effector. In the coding, the motion command and current position were checked. When it is reached 20% of the motion, the next motion command was sent and the motion is start to interpolate to the next command. To give time to the servo driver to interpolate to the next motion, the end velocity and initial velocity selected minimum as 0. This keeps the deceleration and acceleration duration long. This means that the time to adjust the speeds of the servo motors to the next motion was maximized.

6.3.2.3 Path Generation

The code requires the corners of the print path. After the path was determined, the corner points will be entered into the code. The path was divided into smaller parts as 25 mm for the software to calculate the required cable lengths on the path for the end-effector. The code also extrudes the path automatically to add more layers of the same path. Then, these cable lengths for each joint were put in a matrix to be used on the motion. The motion matrix contained the cable lengths of each joint in the first 8 columns and the pose of the end effector for the next 6 columns. There was also a home position for the robot to go before each run. The robot also went from the home position to the beginning of the print path. Every motion requires its own motion matrix with the same structure. The motion code uses the first 8 values of the motion matrices. The pose information was for the operator to keep track of the end-effector.

6.3.3 End-Effector Path Tracking Results

To qualify the performance of the end=effector path tracking, the pose of the end-effector was recorded by OptiTrack IR motion tracking cameras. 7 cameras were attached to the frame of the CDPR in a crescent configuration in two layers. Motion

capture cameras and mounting locations can be seen in Figure 29. The system was calibrated following the manufacturer's procedure. The mean 3D RMSE for camera calibration was 0.276 mm and the mean 2D RMSE was 0.098 pixels. Reflective balls were placed on the end-effector.

The end-effector was given a circular trajectory that has a 0.5 m radius. The trajectory was located at the center line of the workspace and at 0.2 m height, [x,y,z] = [0, 0, 0.2] m. The path tracking has repeated 10 times. The trajectory and motion capture results can be seen in Figure 30. The RMSE for the circular path was 3.69 mm. The close-up result of the circular trajectory can be seen in Figure 31. The RMSE in the x-direction was 3.15 mm and the y-direction was 1.75 mm. Detailed results can be seen in Figure 35.

Considering the 1-meter-diameter path followed during printing, this level of error is adequately acceptable. The necessary sensitivity for concrete printing, which is less than 5 mm, proves sufficient for producing acceptable prints in the concrete printing tests [61].

Also, a square path with a 0.5 m edge length trajectory was followed. The square path was located at the center line of the workspace and at 0.2m height, [x,y,z] = [0, 0, 0.2] m. The path tracking was repeated 10 times. The path that the robot followed can be seen in Figure 32. The trajectory and motion capture results can be seen in Figure 33. The RMSE for the square path was 3.60 mm. The close-up result of a corner of the square trajectory can be seen in Figure 34. The RMSE in the x-direction was 2.74 mm and the y-direction was 2.48 mm. Detailed results can be seen in Figure 36.

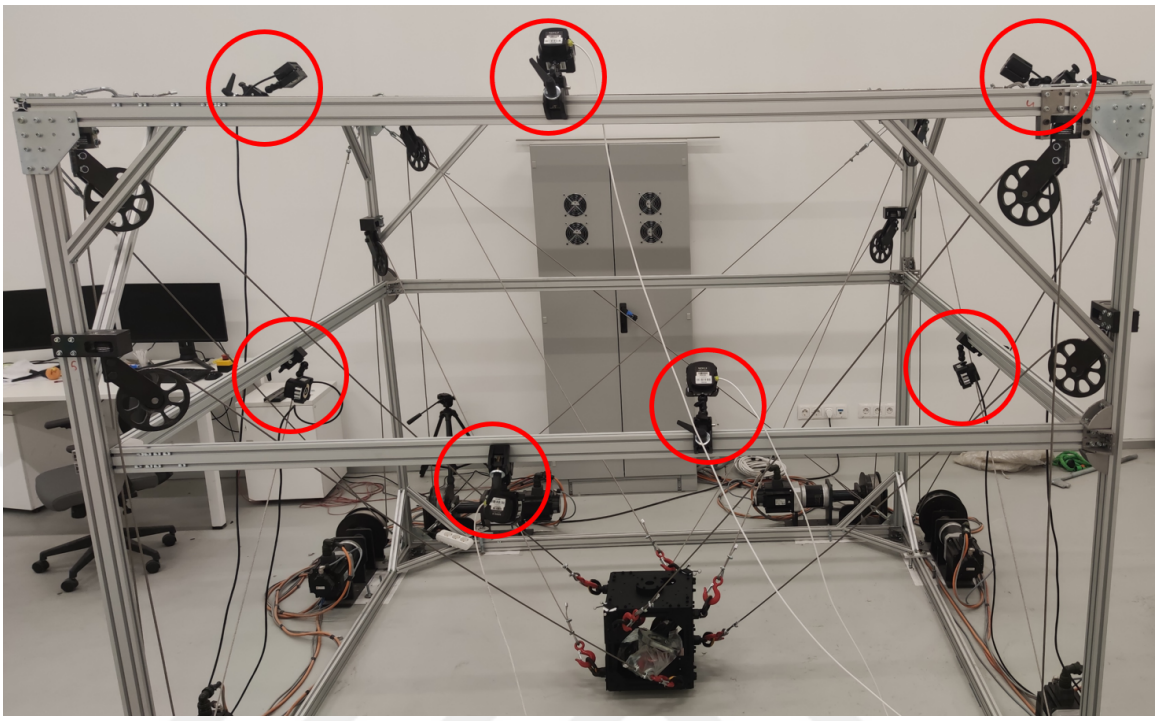

Figure 29: Motion Capture with 7 Cameras

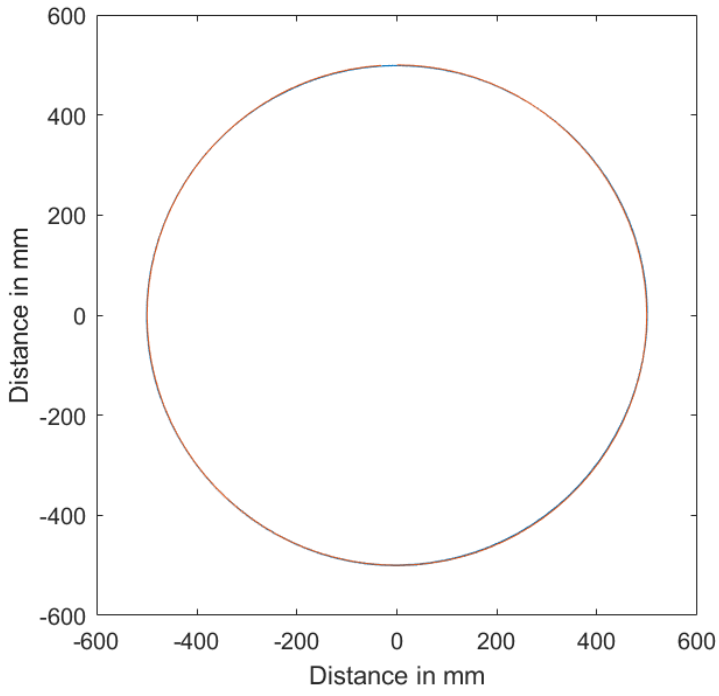

Figure 30: Trajectory and Motion Capture Results of 10 Circle Motion

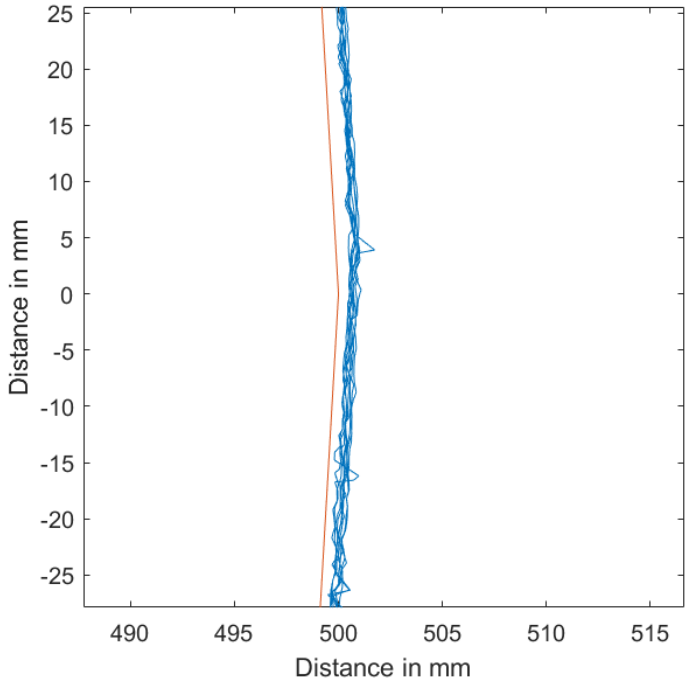

Figure 31: Close-up Circular Trajectory and Motion Capture Results of 10 Circular Motion

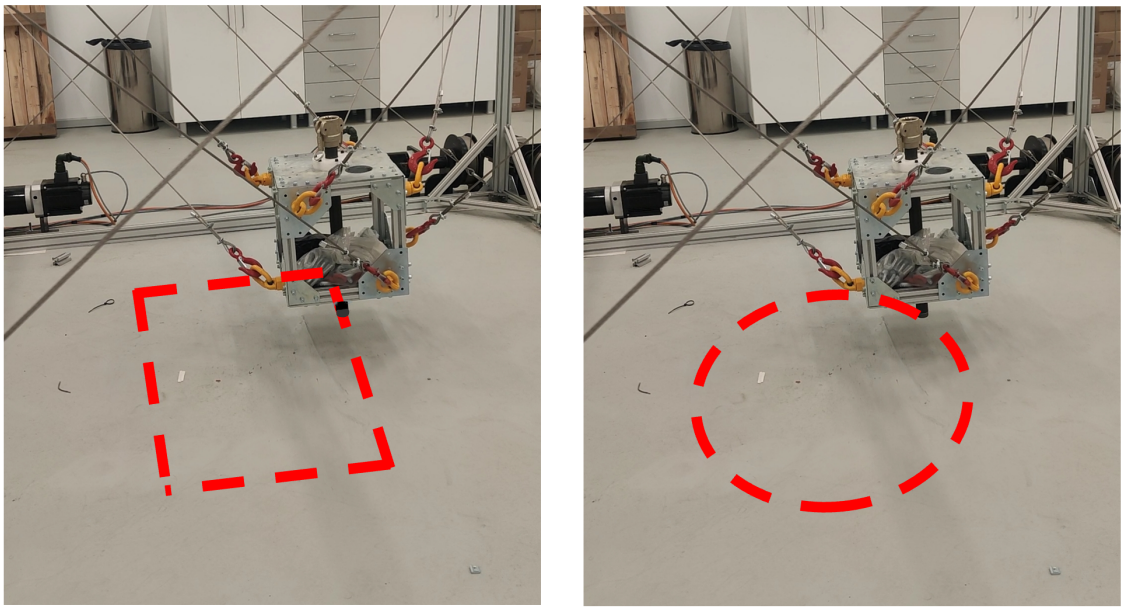

Figure 32: End-Effector Trajectory of Square and Circular Motion Respectively

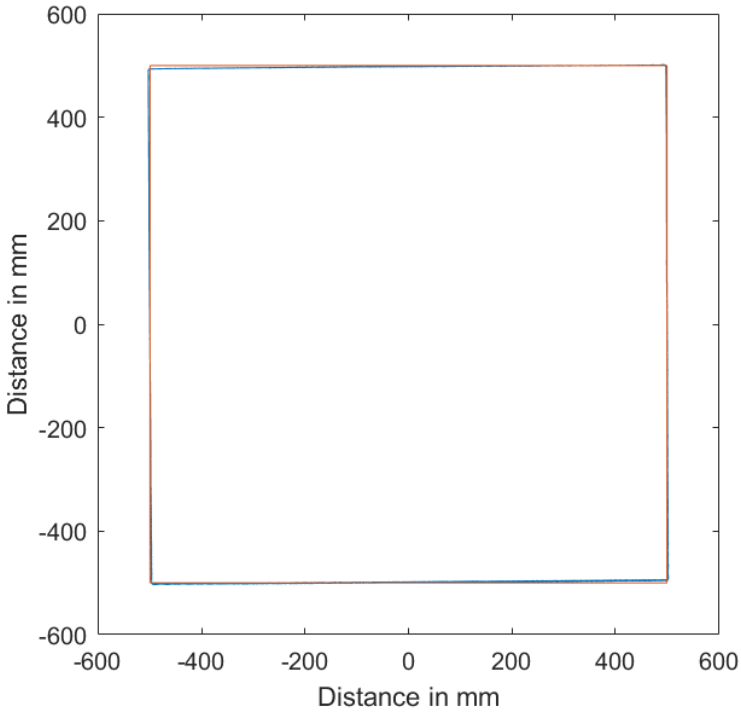

Figure 33: Trajectory and Motion Capture Results of 10 Square Motion

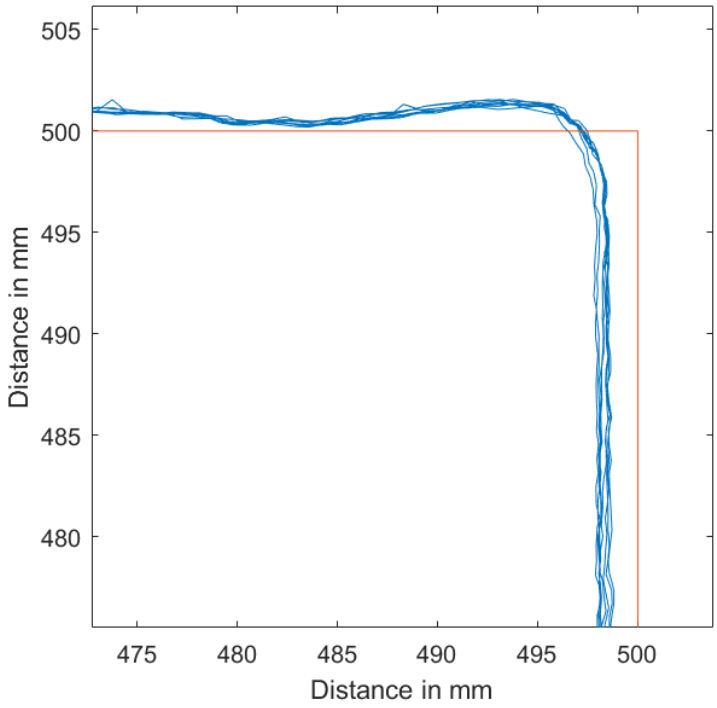

Figure 34: Close-up Square Trajectory and Motion Capture Results of 10 Square Motion

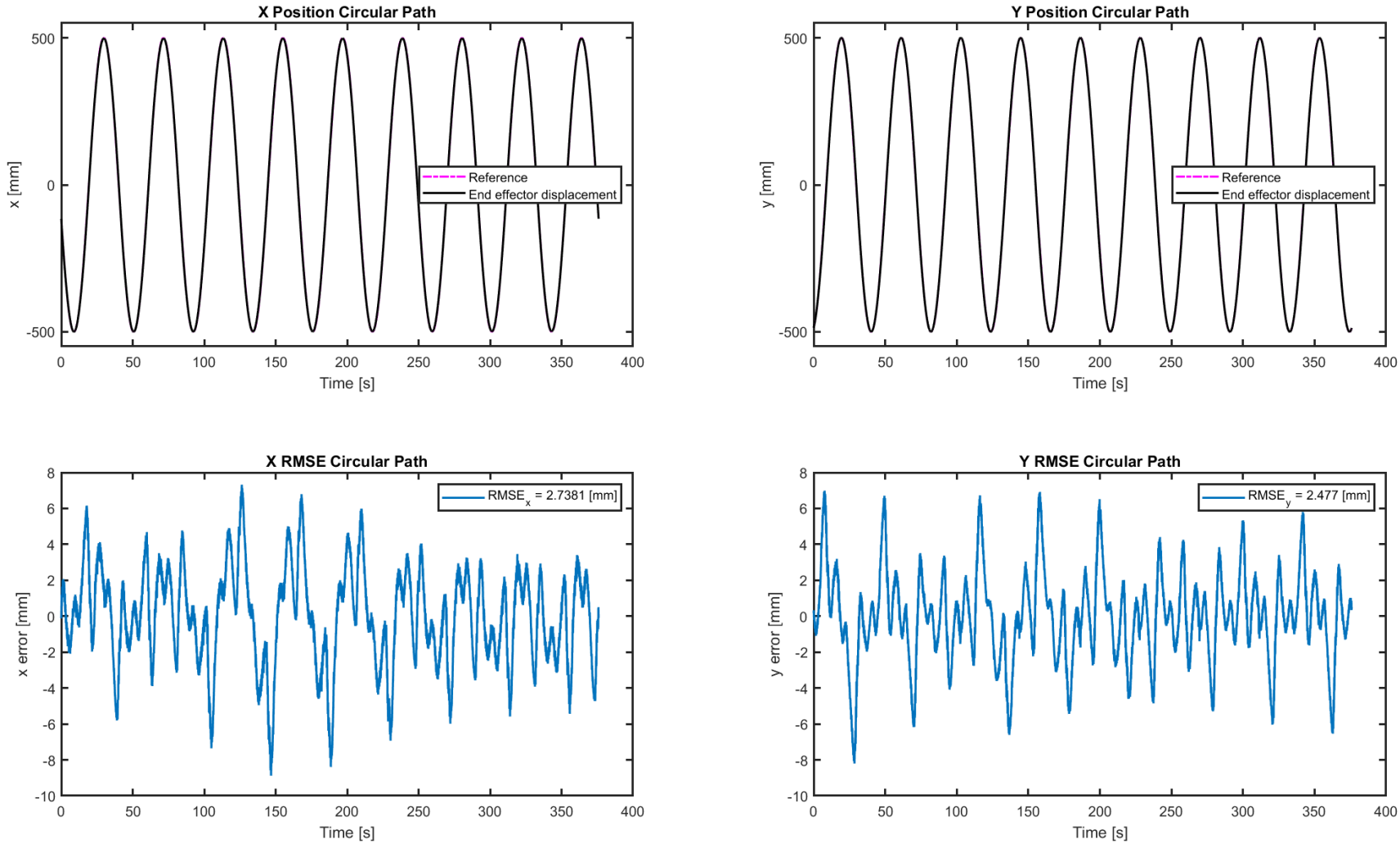

Figure 35: Trajectory result of the circular path and RMSE

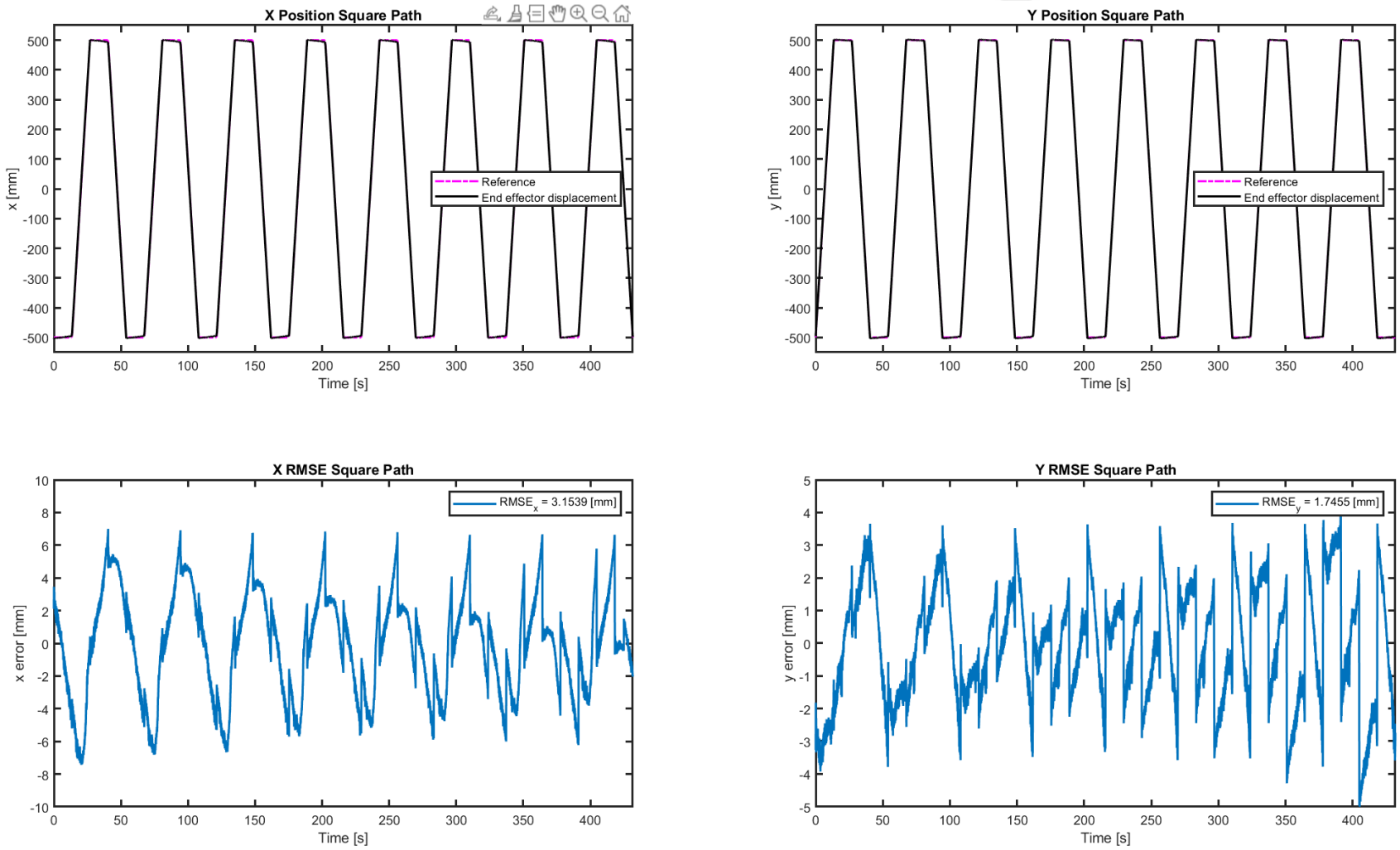

Figure 36: Trajectory result of the square path and RMSE

CHAPTER VII

CONCLUSIONS

Cable-driven parallel robots have recently attracted much interest due to their large workspace and heavy payload capacities. For the same reasons, CDPRs are lately gained interest in additive manufacturing. With the large workspaces, CDPRs can be used to print larger parts. However, the issue is that the large workspace requires longer cables. Long cables are more prone to external forces which reduces the stiffness of the end effector. There are studies on workspace analysis of the CDPRs. There are also studies on the stiffness of the end-effectors of CDPRs. However, there are not enough studies that link workspace and stiffness together.

In this thesis, a novel methodology was proposed to find the relation between the stiffness of a CDPR and the workspace. The methodology uses a novel index called End-Effector Compliance Index (ECI). ECI uses cable direction vectors and cable lengths to qualify the stiffness of the end-effector. ECI is a purely geometrical property of the different poses of an end-effector. The ECI will change with changing pose of an end-effector. In the proposed methodology, the ECI was compared with the cable tension values to determine the distance between anchor point locations for the cables. This methodology was tested on simulations for both suspended and constrained CDPRs with different print parts to find out the difference between suspended and constrained CDPRs. According to the results of the simulations, two formulas were found for deciding a CDPR size for different print parts for both constrained and suspended CDPRs.

The formula for suspended CDPRs was used in a case study. In this study, a suspended CDPR was built for a 1 m print part base length. The CDPR size was

decreased by 1/4 of what the formula suggests to increase the stiffness of the end-effector. This also increased the required cable tensions. The CDPR parts were designed and machined. By using the parts, the CDPR was constructed. The design and construction procedures were explained. The robot's path-tracking results were gathered by using visual motion capture methods. According to the results, the oscillation of the robots on a trajectory is around 1% which is sufficient for additive manufacturing. The stiffness of the end-effector can be increased by doing better cable homing.

REFERENCES

[1] F. Xie, W. Shang, B. Zhang, S. Cong, and Z. Li, "High-precision trajectory tracking control of cable-driven parallel robots using robust synchronization," *IEEE Transactions on Industrial Informatics*, vol. 17, no. 4, pp. 2488–2499, 2021.

[2] H. Hussein, J. C. Santos, and M. Gouttefarde, "Geometric optimization of a large scale cdpr operating on a building facade," in *2018 IEEE/RSJ International Conference on Intelligent Robots and Systems (IROS)*, pp. 5117–5124, 2018.

[3] M. Carricato and J.-P. Merlet, "Stability analysis of underconstrained cable-driven parallel robots," *IEEE Transactions on Robotics*, vol. 29, no. 1, pp. 288–296, 2013.

[4] E. Idà, T. Bruckmann, and M. Carricato, "Rest-to-rest trajectory planning for underactuated cable-driven parallel robots," *IEEE Transactions on Robotics*, vol. 35, no. 6, pp. 1338–1351, 2019.

[5] D. Q. Nguyen and M. Gouttefarde, *Stiffness Matrix of 6-DOF Cable-Driven Parallel Robots and Its Homogenization*, pp. 181–191. Cham: Springer International Publishing, 2014.

[6] X. Jiang, E. Barnett, and C. Gosselin, "Periodic trajectory planning beyond the static workspace for 6-dof cable-suspended parallel robots," *IEEE Transactions on Robotics*, vol. 34, no. 4, pp. 1128–1140, 2018.

[7] Z. Cui, X. Tang, S. Hou, and H. Sun, "Research on controllable stiffness of redundant cable-driven parallel robots," *IEEE/ASME Transactions on Mechatronics*, vol. 23, no. 5, pp. 2390–2401, 2018.

[8] H. R. Fahham and M. Farid, "Optimum design of planar redundant cable-suspended robots for minimum time trajectory tracking," in *ICCAS 2010*, pp. 2156–2163, 2010.

[9] J. Lamaury and M. Gouttefarde, "Control of a large redundantly actuated cable-suspended parallel robot," in *IEEE International Conference on Robotics and Automation*, pp. 4659–4664, 2013.

[10] D. Q. Nguyen, M. Gouttefarde, O. Company, and F. Pierrot, "On the analysis of large-dimension reconfigurable suspended cable-driven parallel robots," in *2014 IEEE International Conference on Robotics and Automation (ICRA)*, pp. 5728–5735, 2014.

[11] N. Pedemonte, T. Rasheed, D. Marquez-Gamez, P. Long, É. Hocquard, F. Babin, C. Fouché, G. Caverot, A. Girin, and S. Caro, "Fastkit: A mobile cable-driven parallel robot for logistics," *Advances in Robotics Research: From Lab to Market: ECHORD++: Robotic Science Supporting Innovation*, pp. 141–163, 2020.

[12] W.-J. Shiang, D. Cannon, and J. Gorman, "Dynamic analysis of the cable array robotic crane," in *Proceedings 1999 IEEE International Conference on Robotics and Automation*, vol. 4, pp. 2495–2500, 1999.

[13] M. Gouttefarde and C. Gosselin, "Analysis of the wrench-closure workspace of planar parallel cable-driven mechanisms," *IEEE Transactions on Robotics*, vol. 22, no. 3, pp. 434–445, 2006.

[14] D. Gueners, H. Chanal, and B. C. Bouzgarrou, "Stiffness optimization of a cable driven parallel robot for additive manufacturing," in *IEEE International Conference on Robotics and Automation (ICRA)*, pp. 843–849, 2020.

[15] P. Liu and H. Ma, "On the stability for a cable-driven parallel robot while considering the cable sag effects," in *2016 13th Int. Conf. on Ubiquitous Robots and Ambient Intelligence (URAI)*, pp. 538–543, 2016.

[16] A. Singh, C. Sahoo, and D. R. Parhi, "Design of a planar cable driven parallel robot using the concept of capacity margin index," in *IEEE 9th Int. Conf. on Intelligent Systems and Control (ISCO)*, pp. 1–7, 2015.

[17] S. Tadokoro, S. Nishioka, T. Kimura, M. Hattori, T. Takamori, and K. Maeda, "On fundamental design of wire configurations of wire-driven parallel manipulators with redundancy," in *Proceedings of the 1996 Japan-USA Symposium on Flexible Automation. Part 2 (of 2)*, pp. 151–158, 1996.

[18] M. Gouttefarde, J.-F. Collard, N. Riehl, and C. Baradat, "Geometry selection of a redundantly actuated cable-suspended parallel robot," *IEEE Transactions on Robotics*, vol. 31, no. 2, pp. 501–510, 2015.

[19] J. Pusey, A. Fattah, S. Agrawal, E. Messina, and A. Jacoff, "Design and workspace analysis of a 6-6 cable-suspended parallel robot," in *Proceedings 2003 IEEE/RSJ International Conference on Intelligent Robots and Systems (IROS 2003)*, vol. 3, pp. 2090–2095, 2003.

[20] J.-A. Seon, S. Park, S. Y. Ko, and J.-O. Park, "Cable configuration analysis to increase the rotational range of suspended 6-dof cable driven parallel robots," in *2016 16th International Conference on Control, Automation and Systems (ICCAS)*, pp. 1047–1052, 2016.

[21] A. Pott, C. Meyer, and A. Verl, "Large-scale assembly of solar power plants with parallel cable robots," in *ISR 2010 (41st International Symposium on Robotics) and ROBOTIK 2010 (6th German Conference on Robotics)*, pp. 1–6, 2010.

[22] H. Wang, J. Kinugawa, and K. Kosuge, "Exact kinematic modeling and identification of reconfigurable cable-driven robots with dual-pulley cable guiding mechanisms," *IEEE/ASME Transactions on Mechatronics*, vol. 24, no. 2, pp. 774–784, 2019.

[23] J. Hanafie, L. Nurahmi, S. Caro, and B. Pramujati, "Design optimization of spatial four cables suspended cable driven parallel robot for rapid life-scan," *AIP Conference Proceedings*, vol. 1983, p. 060007, 07 2018.

[24] A. Yiğit, M. A. Perozo, M. Ouafo, L. Cuvillon, S. Durand, and J. Gangloff, "Aerial manipulator suspended from a cable-driven parallel robot: Preliminary experimental results," in *2021 IEEE/RSJ International Conference on Intelligent Robots and Systems (IROS)*, pp. 9662–9668, 2021.

[25] S. Kawamura and K. Ito, "A new type of master robot for teleoperation using a radial wire drive system," in *Proceedings of 1993 IEEE/RSJ International Conference on Intelligent Robots and Systems (IROS '93)*, vol. 1, pp. 55–60 vol.1, 1993.

[26] H. Jamshidifar, A. Khajepour, B. Fidan, and M. Rushton, "Kinematically-constrained redundant cable-driven parallel robots: Modeling, redundancy analysis, and stiffness optimization," *IEEE/ASME Transactions on Mechatronics*, vol. 22, no. 2, pp. 921–930, 2017.

[27] K. Kozak, Q. Zhou, and J. Wang, "Static analysis of cable-driven manipulators with non-negligible cable mass," *IEEE Transactions on Robotics*, vol. 22, no. 3, pp. 425–433, 2006.

[28] M. Gouttefarde, J.-F. Collard, N. Riehl, and C. Baradat, "Simplified static analysis of large-dimension parallel cable-driven robots," in *2012 IEEE International Conference on Robotics and Automation*, pp. 2299–2305, 2012.

[29] S. Fang, D. Franitza, M. Torlo, F. Bekes, and M. Hiller, "Motion control of a tendon-based parallel manipulator using optimal tension distribution," *IEEE/ASME Transactions on Mechatronics*, vol. 9, no. 3, pp. 561–568, 2004.

[30] L. Mikelsons, T. Bruckmann, M. Hiller, and D. Schramm, "A real-time capable force calculation algorithm for redundant tendon-based parallel manipulators," in *2008 IEEE International Conference on Robotics and Automation*, pp. 3869–3874, IEEE, 2008.

[31] M. Gouttefarde, J. Lamaury, C. Reichert, and T. Bruckmann, "A versatile tension distribution algorithm for n -dof parallel robots driven by $n + 2$ cables," *IEEE Transactions on Robotics*, vol. 31, no. 6, pp. 1444–1457, 2015.

[32] P. H. Borgstrom, B. L. Jordan, G. S. Sukhatme, M. A. Batalin, and W. J. Kaiser, "Rapid computation of optimally safe tension distributions for parallel cable-driven robots," *IEEE Transactions on Robotics*, vol. 25, no. 6, pp. 1271–1281, 2009.

[33] P. Miermeister and A. Pott, "Auto calibration method for cable-driven parallel robots using force sensors," in *Latest Advances in Robot Kinematics* (J. Lenarcic and M. Husty, eds.), (Dordrecht), pp. 269–276, Springer Netherlands, 2012.

[34] X. Jin, J. Jung, S. Y. Ko, E. Choi, J.-O. Park, and C.-S. Kim, "Geometric parameter calibration for a cable-driven parallel robot based on a single one-dimensional laser distance sensor measurement and experimental modeling," *Sensors*, vol. 18, no. 7, p. 2392, 2018.

[35] H. Yuan, E. Courteille, and D. Deblaise, "Static and dynamic stiffness analyses of cable-driven parallel robots with non-negligible cable mass and elasticity," *Mechanism and Machine Theory*, vol. 85, pp. 64–81, 2015.

[36] R. Meziane, P. Cardou, and M. J.-D. Otis, "Cable interference control in physical interaction for cable-driven parallel mechanisms," *Mechanism and Machine Theory*, vol. 132, pp. 30–47, 2019.

[37] X. Weber, L. Cuvillon, and J. Gangloff, "Active vibration canceling of a cable-driven parallel robot in modal space," in *2015 IEEE International Conference on Robotics and Automation (ICRA)*, pp. 1599–1604, 2015.

[38] J.-P. Merlet, "The kinematics of cable-driven parallel robots with sagging cables: preliminary results," in *2015 IEEE International Conference on Robotics and Automation (ICRA)*, pp. 1593–1598, 2015.

[39] O. Bohigas, M. Manubens, and L. Ros, "Planning wrench-feasible motions for cable-driven hexapods," *IEEE Transactions on Robotics*, vol. 32, no. 2, pp. 442–451, 2016.

[40] N. Zhang, W. Shang, and S. Cong, "Dynamic trajectory planning for a spatial 3-dof cable-suspended parallel robot," *Mechanism and Machine Theory*, vol. 122, pp. 177–196, 2018.

[41] X. Jiang and C. Gosselin, "Dynamic point-to-point trajectory planning of a three-dof cable-suspended parallel robot," *IEEE Transactions on Robotics*, vol. 32, no. 6, pp. 1550–1557, 2016.

[42] L. Kevac, M. Filipovic, and A. Rakic, "The trajectory generation algorithm for the cable-suspended parallel robot—the cpr trajectory solver," *Robotics and Autonomous Systems*, vol. 94, pp. 25–33, 2017.

[43] P. Miermeister and A. Pott, "Modelling and real-time dynamic simulation of the cable-driven parallel robot ipanema," in *New Trends in Mechanism Science*, (Dordrecht), pp. 353–360, Springer Netherlands, 2010.

[44] P. Borgstrom, P. Borgstrom, M. Stealey, B. Jordan, G. Sukhatme, M. Batalin, and W. Kaiser, "Design and implementation of nims3d, a 3-d cabled robot for actuated sensing applications," *Robotics, IEEE Transactions on*, vol. 25, pp. 325 – 339, 05 2009.

[45] J. K. Pickard, J. A. Carretero, and V. C. Bhavsar, "Task-optimized cable-actuated planar parallel manipulator architecture and its concurrent implementation," in *2014 International Conference on High Performance Computing Simulation (HPCS)*, pp. 178–185, 2014.

[46] L. Gagliardini, S. Caro, and M. Gouttefarde, "Dimensioning of cable-driven parallel robot actuators, gearboxes and winches according to the twist feasible workspace," in *2015 IEEE International Conference on Automation Science and Engineering (CASE)*, pp. 99–105, 2015.

[47] M. Arsenault, "Optimization of the prestress stable wrench closure workspace of planar parallel three-degree-of-freedom cable-driven mechanisms with four cables," in *2010 IEEE International Conference on Robotics and Automation*, pp. 1182–1187, 2010.

[48] M. Gouttefarde, J.-P. Merlet, and D. Daney, "Wrench-feasible workspace of parallel cable-driven mechanisms," in *Proceedings 2007 IEEE International Conference on Robotics and Automation*, pp. 1492–1497, 2007.

[49] L. Gagliardini, S. Caro, M. Gouttefarde, P. Wenger, and A. Girin, "Optimal design of cable-driven parallel robots for large industrial structures," in *2014 IEEE International Conference on Robotics and Automation (ICRA)*, pp. 5744–5749, 2014.

[50] A. Ghasemi, M. Eghtesad, and M. Farid, "Workspace analysis of planar and spatial redundant cable robots," in *2008 American Control Conference*, pp. 2389–2394, 2008.

[51] X. Wang and S. Bhattacharya, "A topological approach to workspace and motion planning for a cable-controlled robot in cluttered environments," *IEEE Robotics and Automation Letters*, vol. 3, no. 3, pp. 2600–2607, 2018.

[52] T. Rasheed, P. Long, and S. Caro, "Wrench-feasible workspace of mobile cable-driven parallel robots," *Journal of Mechanisms and Robotics*, vol. 12, pp. 1–23, 11 2019.

[53] G. Yang, C. B. Pham, and S. H. Yeo, "Workspace performance optimization of fully restrained cable-driven parallel manipulators," in *2006 IEEE/RSJ International Conference on Intelligent Robots and Systems*, pp. 85–90, 2006.

[54] D. Zanotto, G. Rosati, S. Minto, and A. Rossi, "Sophia-3: A semiadaptive cable-driven rehabilitation device with a tilting working plane," *IEEE Transactions on Robotics*, vol. 30, no. 4, pp. 974–979, 2014.

[55] J.-P. Merlet, "Singularity of cable-driven parallel robot with sagging cables: Preliminary investigation," in *2019 International Conference on Robotics and Automation (ICRA)*, pp. 504–509, 2019.

[56] S. Lessanibahri, P. Cardou, and S. Caro, "Parasitic Inclinations in Cable-Driven Parallel Robots using Cable Loops," in *The 28th CIRP Design Conference*, vol. 70, (Nantes, France), pp. 296–301, May 2018.

[57] Y. Qiu, B. Duan, Q. Wei, and J. Du, "Elimination of force singularity of the cable and cabin structure for the next generation large radio telescope," *Mechatronics*, vol. 12, no. 7, pp. 905–918, 2002.

[58] W. Shang, B. Zhang, B. Zhang, F. Zhang, and S. Cong, "Synchronization control in the cable space for cable-driven parallel robots," *IEEE Transactions on Industrial Electronics*, vol. 66, no. 6, pp. 4544–4554, 2019.

[59] Z. Zake, F. Chaumette, N. Pedemonte, and S. Caro, "Vision-based control and stability analysis of a cable-driven parallel robot," *IEEE Robotics and Automation Letters*, vol. 4, no. 2, pp. 1029–1036, 2019.

[60] R. Mersi, S. Vali, M. S. haghighi, G. Abbasnejad, and M. T. Masouleh, "Design and control of a suspended cable-driven parallel robot with four cables," in *2018 6th RSI International Conference on Robotics and Mechatronics (IcRoM)*, pp. 470–475, 2018.

[61] T. P. Tho and N. T. Thinh, "Using a cable-driven parallel robot with applications in 3d concrete printing," *Applied Sciences*, vol. 11, no. 2, p. 563, 2021.

[62] M. Banciu, "Dual simplex," in *Wiley Encyclopedia of Operations Research and Management Science*, Wiley, 2011.

[63] D. Zanotto, G. Rosati, and A. Rossi, "Performance analysis of planar cable-based parallel manipulators," in *Engineering Systems Design and Analysis*, vol. 49170, pp. 789–798, 2010.

[64] S. Abdolshah, D. Zanotto, G. Rosati, and S. K. Agrawal, "Optimizing stiffness and dexterity of planar adaptive cable-driven parallel robots," *Journal of Mechanisms and Robotics*, vol. 9, no. 3, p. 031004, 2017.

[65] K. Feyrer, *Wire ropes*. Springer, 2007.

[66] P. Marshall, "Austenitic stainless steels: microstructure and mechanical properties," p. 27, 1984.

VITA

Ahmet Burhan Kara was a student in B.Sc and M.Sc. programs in mechanical engineering at Özyeğin University, Türkiye. He worked as a student assistant at the Robotic Laboratory under the supervision of Asst. Prof. Özkan Bebek and Assoc. Prof. Zeynep Başaran Bundur. Besides his tasks such as assistance in Solid Mechanics, Mechanical Design, and Industrial Robot Programming, he designed, constructed, and controlled a cable-driven parallel robot. He also worked on an industrial robotic arm and a solenoid-based injector. He had roles in two industrial collaboration projects. He published four journals and three conference papers. He's familiar with the fundamentals of part design, machining techniques, additive manufacturing, and industrial servo control.